

1 **Dissolved concentrations and organic speciation of copper in the Amazon**

2 **River estuary and mixing plume**

3

4 Adrienne Patricia Hollister^{1*}, Hannah Whitby², Michael Seidel³, Pablo Lodeiro^{4,5}, Martha
5 Gledhill⁴, Andrea Koschinsky¹

6

7 *Corresponding author: Adrienne Patricia Hollister (a.hollister@jacobs-university.de)

8

9 ¹Jacobs University Bremen gGmbH, Campus Ring 1, 28759 Bremen, Germany

10 ²School of Environmental Sciences, University of Liverpool, Liverpool, L69 3GP, UK

11 ³Institute for Chemistry and Biology of the Marine Environment, University of
12 Oldenburg, Carl-von-Ossietzky-Str. 9-11, 26129 Oldenburg, Germany

13 ⁴GEOMAR Helmholtz Centre for Ocean Research Kiel, 24148 Kiel, Germany;

14 ⁵Department of Chemistry , University of Lleida – AGROTECNIO-CERCA Center, Rovira
15 Roure 191, 25198, Lleida, Spain

16

Abstract

The Amazon is Earth's largest river by volume output, making it an important source of trace metals and dissolved organic matter (DOM) to the Atlantic Ocean. Despite major recent anthropogenic disruptions to the Amazon catchment area, data for trace metals such as copper (Cu) in the Amazon River estuary and associated mixing plume are still rare. Furthermore, there is currently no existing data in this region for Cu-binding ligands, which govern the amount of bioavailable Cu. To understand trace metal mixing and transport processes, the GEOTRACES process study GApr11 (cruise M147 with *RV Meteor*) was conducted in 2018 in the Amazon and Pará River estuaries and mixing plume in the tropical North Atlantic Ocean during high river discharge. Size-fractionated surface samples were collected along the full salinity gradient for concentrations of Cu, apparent Cu-binding organic ligands (L_{Cu}) and corresponding conditional stability constants ($K'^{cond}_{CuL,Cu2+}$), electroactive humic substances (eHS), solid phase extractable organic Cu (SPE-Cu), dissolved organic carbon (DOC), chlorophyll *a* (Chl *a*) and macronutrients. Dissolved ($<0.2 \mu m$) and soluble ($<0.015 \mu m$) Cu correlated negatively with salinity and largely followed values expected from conservative mixing. Cu was primarily in the soluble fraction, with the exception of a minor fraction of large colloidal Cu at low salinity ($S \leq 10$). Organic ligands ($\log K'^{cond}_{CuL,Cu2+} = 12.6-15.6$) were present in excess of Cu and likely played a role in solubilizing Cu and preventing Cu being affected by colloidal flocculation. Cu-associated DOM (measured as L_{Cu} , eHS and SPE-Cu) correlated negatively with salinity and appeared to be primarily governed by river input and mixing with seawater. However, an increase in the colloidal fraction for L_{Cu} and eHS

39 observed at S ~6-10 was attributed to possible additional autochthonous
40 (phytoplankton) ligand production. In all dissolved samples, organic complexation kept
41 free Cu below levels potentially toxic for phytoplankton ($<1 \text{ pmol L}^{-1}$). Despite increasing
42 anthropogenic activity over the past century, we find Cu concentrations remained
43 similar to the 1970s, suggesting that the large overall river flow may so far minimize the
44 impact of Cu pollution.

1. Introduction

The Amazon River is the largest on Earth, accounting for 15 - 20% of all freshwater input to the ocean, making it a major source of trace metals, macronutrients and dissolved organic matter (DOM) to the Atlantic Ocean (Meybeck 1982; Richey et al. 1986; Smoak et al. 2006; Villar et al. 2009). The Amazon region experiences distinct wet (January to August) and dry (September to December) seasons, which affect river flow rate ($100\,200 - 240\,000\text{ m}^3\text{ s}^{-1}$ at station Óbidos) (Richey et al. 1986; Villar et al. 2009) and residence time (estimated 14 - 22 days in the Santana Channel; de Abreu et al. 2020). In addition to the Amazon River, the estuarine mixing zone is also influenced by outflow from the Pará River and its main tributary the Tocantins River (average flow $11\,000\text{ m}^3\text{ s}^{-1}$; Costa et al. 2003) and catchment area to the south. Finally, a large mangrove forest to the southeast of the Pará River outflow provides a source of nutrient- and DOM-rich groundwater (Dittmar and Lara 2001). Due to its enormous volume, water from the Amazon and Pará River estuaries is pushed onto the continental shelf. Here, the brackish water mixes with entrainment of offshore water from the North Brazil Current (NBC), which is further influenced by large tidal fluctuations (Smoak et al. 2006).

Copper (Cu) is an important marine trace metal that is required for a variety of enzymes involved in electron transport (Sunda 2012) and is sometimes a co-limiting nutrient along with iron (Fe) (Peers et al. 2005; Annett et al. 2008; Semeniuk et al. 2009). However, Cu can also be toxic to phytoplankton; free Cu can reduce the growth rate of cyanobacteria at concentrations $>1\text{ pmol L}^{-1}$ and eukaryotic phytoplankton at concentrations $>10\text{ pmol L}^{-1}$ (Brand et al. 1986). This toxicity is mitigated by a high

degree of organic complexation (>99%), which greatly decreases the concentration of free Cu (van den Berg et al. 1987; Coale and Bruland 1988; Buck and Bruland 2005; Moffett and Dupont 2007; Jacquot and Moffett 2015; Whitby et al. 2017).

Several studies have observed a conservative-type trend for Cu in estuaries governed primarily by river-seawater mixing (Boyle et al. 1982; Windom et al. 1988; Abdel-Moati 1990; Cutter 1991; Zhang 1995; Illuminati et al. 2019), although deviations from this overall conservative behavior may result from sorption to solids, colloidal flocculation and/or biological uptake (Boyle et al. 1982; Abdel-Moati 1990; Tang et al. 2002; Pearson et al. 2017; Dulaquais et al. 2020; Pavoni et al. 2020). Changes in the chemical speciation and size fractionation of Cu can also reflect the dynamic processes that occur within estuarine plumes. Colloidal flocculation of trace metals can play a major role in the removal of a variety of potentially toxic metals, including Cu, during estuarine mixing (Heidari 2019). Moreover, the thermodynamic properties of DOM are crucial to understanding trace metal binding behavior (Lodeiro et al. 2020). Therefore, size fractionation and ligand concentration and binding strength are important factors in governing Cu concentration and bioavailability in estuaries.

The organic ligands responsible for Cu complexation can be analyzed using indirect electrochemical methods, which measure the ligand pool based on concentration and binding strength. Organic Cu-binding ligands (L_{Cu}) are commonly grouped based on binding strength into stronger (L1) and weaker (L2) ligand classes, with the majority of dissolved Cu bound to L1 (Coale and Bruland 1988; Buck and Bruland 2005; Whitby et al. 2017; Whitby et al. 2018). These ligands can be produced by

phytoplankton in response to Cu toxicity (Moffett and Brand 1996; Leal et al. 1999), as well as being released during phytoplankton degradation (Lorenzo et al. 2007) or generated as metabolic byproducts (Laglera and Tovar-Sánchez 2012). In addition, Cu-reactive humic substances, including humic and fulvic acids, make up a large fraction of the natural, terrestrially-derived DOM and are therefore especially important in estuarine regions (Mantoura et al. 1978; Kogut and Voelker 2001; Voelker and Kogut 2001; Shank et al. 2004; Whitby et al. 2017; Dulaquais et al. 2020).

Cu-binding ligands in estuaries play an important role in mitigating Cu toxicity and bioavailability. These ligands, which include reduced sulfur species (RSS) such as thiols as well as humic substances, have been reported across a range in binding strengths from $\log K'_{CuL,Cu2+}^{cond} \sim 10 - 16$ (van den Berg et al. 1987; Tang et al. 2001; Laglera and van den Berg 2003; Buck and Bruland 2005; Dryden et al. 2007; Santos-Echeandía et al. 2013; Whitby et al. 2017; Wong et al. 2019). Humic-like substances account for up to estimated 40 - 60% of dissolved organic carbon (DOC) in aquatic environments (McKnight and Aiken 1998; Zigah et al. 2017), and contribute up to 60% of the DOC transported by the Amazon River (Ertel et al. 1986). In addition, humic-like ligands have been detected throughout the coastal and open ocean (Laglera and van den Berg 2009; Whitby and van den Berg 2015; Dulaquais et al. 2018; Whitby et al. 2018; Whitby et al. 2020). Because of the high diversity of humic-like substances, these ligands are often quantified by voltammetric analyses (Whitby and van den Berg 2015; Whitby et al. 2017; Whitby et al. 2018). These operationally-defined electroactive humic substances (eHS) are a useful proxy for the pool of Cu-binding humic ligands. Solid phase extraction (SPE)

provides an additional way to analyze hydrophobic DOM-associated Cu in greater detail (Waska et al. 2015; Boiteau et al. 2016), which comprises a substantial portion (~10 - 50%) of estuarine dissolved Cu (Elbaz-Poulichet et al. 1994; Beck et al. 2010). Taken together, electrochemical analyses of L_{Cu} and eHS, combined with SPE, provide a suite of tools to evaluate Cu-associated DOM in estuaries and seawater.

Research in the Amazon River estuary and plume conducted in the 1970s showed that Cu concentrations generally followed a distribution expected from conservative mixing, with evidence of additional biological uptake during slower plume circulation (Boyle et al. 1982). However, more recent observations of Cu and other trace metals in the Amazon are sparse and have focused primarily on the mixing and transport in Amazon River tributaries prior to reaching the Atlantic Ocean (Aucour et al. 2003; Seyler and Boaventura 2003; Guinoiseau et al. 2018). Furthermore, to our knowledge, no study of Cu size partitioning (dissolved, colloidal and soluble) has been conducted in the Amazon Estuary.

Since the Boyle et al. (1982) study, the Amazon River basin has been subjected to a variety of anthropogenic impacts, including agriculture, deforestation, mining and hydroelectric dams (Coe et al. 2009; Davidson et al. 2012). Climate change is also expected to alter precipitation over the entire Amazon River basin (Guimberteau et al. 2013), resulting in both flooding and drought in different regions, and therefore impacting trace metal fluxes from the Amazon region into the coastal Atlantic Ocean. Because of the importance of trace metals in governing marine primary productivity and carbon sequestration (see e.g. Morel and Price 2003; Sunda 2012), large disruptions to

the Amazon River could have a profound impact on the Atlantic Ocean as a whole through meridional overturning circulation. To assess the impacts of anthropogenic activity and to support models of future climate-change scenarios, it is therefore critical to understand the geochemistry of the Amazon River estuary and surrounding regions of the Northwest Brazilian Continental Shelf.

In this study, we aimed to establish whether the Amazon and Pará Rivers were significant sources of dissolved Cu to the tropical North Atlantic Ocean, and to assess whether a change in Cu concentrations and speciation could impact the ecosystem in coastal and estuarine waters. To this end, we measured Cu and Cu-binding organic matter present in the dissolved ($<0.2\ \mu\text{m}$), soluble ($<0.015\ \mu\text{m}$), and ultrafiltered (<1 and $<10\ \text{kDa}$) fractions. To assess Cu chemical speciation at different salinities and size fractions, we undertook a three-pronged investigation of 1) apparent L_{Cu} concentrations and their associated conditional stability constants, 2) eHS concentrations and 3) hydrophobic Cu concentrations via size exclusion chromatography (SEC). Our results highlight the role of river-derived organic ligands in stabilizing Cu in the study area, with possible additional autochthonous production of large colloidal L_{Cu} in the mid-salinity region.

2. Methods

2.1. Sample collection

A GEOTRACES process study (cruise M147 Amazon-GEOTRACES, GApr11) was completed in the Amazon River estuary and nearby regions of the Northwest Brazilian

Continental Shelf (**Fig. 1a**) during the high river discharge season (29 April to 20 May 2018). Surface samples for concentrations of dissolved Cu, L_{Cu} and eHS were collected aboard the RV Meteor with a towed-fish (2 to 3 m depth) directly into a trace metal-clean laboratory container using a Teflon bellows pump as previously described (Koschinsky et al. 2018; Zhang et al. 2020). Samples for Cu concentration analysis were filtered shipboard into acid-cleaned low-density polyethylene (LDPE) bottles, acidified to pH <2 with Ultrapure HCl (UpA, Romil). Samples were then stored at room temperature for a minimum of one year prior to analysis, since long-term storage (> 2 months) has been found to be necessary to avoid underestimation dissolved Cu concentrations (Posacka et al. 2017). Samples for L_{Cu} and eHS analysis were filtered into acid-cleaned LDPE bottles and stored frozen (-20 °C). To avoid potential contamination from plastic leaching from the towed-fish tubing, samples for SPE analysis were collected from standard Niskin bottles (24 x 12 L, Ocean Test Equipment) deployed on an epoxy coated aluminum rosette equipped with a Seabird SBE 911 plus CTD.

Samples were collected across the full salinity range (0 to >35) (**Fig. 1b**). Salinity data was collected using the ship's sensor in addition to measuring an aliquot of each of the towed-fish trace metal samples after collection, in order to account for the sometimes rapidly-changing salinity during sample collection with a towed-fish. All reported salinity data for towed-fish samples reflect the salinity measured after collection, unless insufficient volume was present, in which case the ship sensor data was used. All samples were filtered shipboard through 0.8/0.2 μ m cartridge filters (AcroPak1000™) to obtain the dissolved fraction. A subset was then further filtered

through acid-cleaned 0.015 μm filter membranes to obtain the soluble fraction as specified; samples for soluble Cu concentrations were filtered through an Anapore filter (Millipore) and samples for soluble L_{Cu} and eHS and were filtered through a Nuclepore Track-Etch filter (Whatman). Both sets of filters were acid washed with 0.1 mol L^{-1} HCl (Suprapur, Merck). The large colloidal fraction (here defined as 0.015 to 0.2 μm) was quantified indirectly by taking the difference between these two size fractions. Four selected samples for dissolved L_{Cu} were also ultrafiltered at 1 and 10 kDa on a Merck Millipore Cross Flow system, and the permeate fraction was saved for analysis. The system was cleaned by circulating 30 mmol L^{-1} HCl (ultrapure, Roth) for 10 minutes after each sample. All sampling and cleaning was performed according to GEOTRACES protocols (<https://geotracesold.sedoo.fr/images/Cookbook.pdf>).

2.2. Chlorophyll *a*, dissolved organic carbon and macronutrient analyses

Dissolved nutrient concentrations (phosphate, nitrate and silicate) were determined on board in samples collected from the towed-fish and from the CTD rosette using a continuous flow auto analyzer (SEAL QuAAtro). Reference materials (Kanso Co, Japan) were analyzed alongside samples in each run as quality control. Samples from salinities <25 were filtered (0.45 μm , 33 mm, polyethersulfone syringe filter, Fisher) to avoid interference from particulate material.

Samples for Chl *a* were collected from the Niskin bottles on an aluminum CTD rosette. Samples were filtered through glass fiber filters (Fisher MF300, 0.7 μm) and the filters frozen at -80°C for shipment and storage. Samples were extracted into 90%

acetone, ultrasonicated, filtered through 0.2 µm PTFE filters (VWR International), diluted where necessary and analyzed for pigments by HPLC with fluorescence and diode array detection according to the method of Van Heukelem and Thomas (2001). We report total Chl *a* concentrations here.

The samples for DOC analysis were filtered with a peristaltic pump using a Causapure pre-filter cartridge (1 µm, polypropylene, Infiltec) and a Causa-PES filter cartridge (0.1 µm, polyethersulfone, Infiltec). The filtration setup was thoroughly rinsed with sample before each use. Triplicates of 30 ml sample were collected in sample-rinsed HDPE (high density polyethylene, Nalgene) vials, acidified to pH 2 (HCl 25%, p.a.) and stored at 4° C until analysis. DOC concentrations were measured by high temperature catalytic combustion on a Shimadzu TOC-VCPH instrument. Precision and accuracy were tested against the Atlantic deep-sea reference sample (D. Hansell, University of Miami, USA) and were better than 5%.

2.3. Cu concentration analysis

Samples were preconcentrated in order of increasing salinity using an automated Elemental Scientific Inc. (ESI) seaFAST system (seaFAST-pico™) prior to analysis by inductively-coupled plasma-mass spectrometry (ICP-MS; Thermo Element XR); for the lowest salinity samples ($S < 1$), no preconcentration was needed, and the samples were analyzed directly on the ICP-MS. Copper concentrations were measured using isotope dilution, as previously described (Rapp et al. 2017). Briefly, acidified seawater samples were spiked with a standard that contained known isotopic ratios. Each sample run was

also accompanied by manifold blanks, seawater quality controls (QCs) and National Research Council Canada (NRC-CNRC) standards CASS 6 and NASS 7 (**Table 1**). Prior to preconcentration, all samples were UV-irradiated for 4 hr in order to destroy existing organic complexation, which can result in incomplete column recovery (Biller and Bruland 2012). Samples were then preconcentrated on a chelating resin (either Wako or Nobias) using the seaFAST as follows. Sample seawater was mixed with ammonium-acetate buffer ($\text{pH } 8.5 \pm 0.05$) to reach a final pH of 6.2 ± 0.05 prior to loading onto the column. The column was rinsed with ultrapure water obtained from a Milli-Q® water purification system (Merck group), with a resistivity of $18.2 \text{ M}\Omega\cdot\text{cm}$ and total organic carbon $<5 \text{ ppb}$, and the trace metals were eluted in 1 mol L^{-1} nitric acid (UpA, Romil) with 1 ppb In as an internal standard. Between samples, the column was rinsed in 1 mol L^{-1} nitric acid without In. Finally, the trace metal counts were measured on the ICP-MS. Counts for ^{63}Cu and ^{65}Cu were normalized to In, the manifold blank counts were subtracted, and the $^{63}\text{Cu}/^{65}\text{Cu}$ ratio was used to determine Cu concentration based on the isotope spike. Uncertainty in Cu values was determined to be 11.2% based on lab values for the NRC standards (**Table 1**) using the Nordtest approach as described in Rapp et al. (2017). To determine concentrations in manifold blanks, which cannot be calculated using isotope spikes, a standard addition curve was used, and the limit of detection (LOD) was determined to be three times the standard deviation of the air blanks ($n = 30$, $\text{LOD} = 5.2 \text{ pmol L}^{-1}$). The riverine end members ($S < 1$) were run directly on the ICP-MS with an isotope spike without seaFAST preconcentration.

2.4. Cu-binding organic ligand analysis

Samples for Cu-speciation were thawed overnight prior to analysis. Organic L_{Cu} concentrations and conditional stability constants ($K'_{CuL,Cu2+}^{cond}$) were analyzed using competitive ligand exchange adsorptive cathodic stripping voltammetry (CLE-AdCSV) (Campos and van den Berg 1994) on a 757 VA Computrace (Metrohm). Each sample was analyzed by measuring a set of 12 - 18 titration points as follows. The dissolved ($<0.2 \mu m$) samples were generally analyzed using a 12-point titration unless otherwise specified (**Supplemental Table S1**) of 0 - 100 nmol L^{-1} added Cu, which included two sample seawater blanks and 10 additions of Cu. For the soluble and ultrafiltered samples, the titration was expanded to 18 points (two blanks, 16 additions of Cu), and the range was decreased to 0 - 60 nmol L^{-1} added Cu to obtain better resolution. Sample seawater (10 mL) was buffered with 70 μL of 0.01 mol L^{-1} ammonium borate buffer to reach a target pH 8.2 and a series of Cu-spikes (0 - 100 nmol L^{-1}) were added in acid-cleaned and pre-conditioned Polytetrafluoroethylene (PTFE; Teflon) pots. The actual pH was checked 3 times distributed evenly throughout the titration, and the average pH value was then used in the calculation for the side reaction coefficient for inorganic Cu ($\alpha_{Cu'}$; **Supplemental Table S1**). The ligand salicylaldoxime (SA) was then added as a competing ligand using established methods (Campos and van den Berg 1994), and the resulting seawater was allowed to sit overnight. An analytical window corresponding to a competing ligand concentration of 10 $\mu mol L^{-1}$ SA was used unless otherwise specified (**Supplemental Table S1**) to ensure a strong ligand class was detected (Bundy et al. 2013; Whitby et al. 2018). Due to limited sample volume, multiple detection windows

could not be used. Each titration point was measured a minimum of 3 times by CLE-AdCSV using a hanging mercury drop electrode (HMDE, Metrohm). The titration curves were fitted using ProMCC (Omanović et al. 2015) to obtain L_{Cu} concentration, $K'^{cond}_{CuL,Cu2+}$ and Cu^{2+} concentration as described in the **Supplemental Information**.

After sample titration, a portion of each sample (30 - 60 mL) was transferred to an acid-cleaned LDPE bottle, acidified (pH <2) with HCl (Suprapur, Merck) and analyzed for trace metals following the methods described in section 2.2. The resulting Cu concentration values (**Supplemental Table S1**) were used in the L_{Cu} titration calculations.

2.5. Electroactive humic substance analysis

The concentrations of eHS were analyzed using cathodic stripping voltammetry of their complexes with Cu (Whitby and van den Berg 2015). The voltammetric apparatus consisted of a μ -Autolab III potentiostat (Ecochemie, Netherlands) connected to a 663 VA stand (Metrohm) with hanging mercury drop electrode (HMDE). The reference electrode was Ag/AgCl with a 3 mol L⁻¹ KCl salt bridge and a glassy carbon counter electrode. Samples were defrosted in the dark at 4 °C and analyzed within 3 days. Before analysis, samples were swirled gently, and 10 mL was added to a glass voltammetric cell with an EPPS buffer (N-(2-hydroxyethyl)piperazine-N'-2-propanesulfonic acid in 1 mol L⁻¹ NH₄; 100 μ L addition to 10 mL seawater buffered the pH to 8.05) and 30 nmol L⁻¹ added Cu (spectrophotometry standard, pH 2). This was purged with nitrogen for up to 5 minutes to remove dissolved oxygen prior to analysis. A

deposition potential of +0.05 V was used, usually for a deposition time of 60s (modified for some samples for all standard additions to remain within the linear range), with a 1s jump to -0.2 V and background subtraction (subtraction of a 1s scan), to improve the baseline and reduce interference from free Cu. Concentrations were analyzed using standard additions of the International Humic Substances Society (IHSS) Suwannee River humic acid (SRHA) standard (II 2S101H).

2.6. Solid phase extraction and analysis

The hydrophobic Cu fraction (SPE-Cu) was extracted onto a modified divinyl-polystyrene solid phase (ENV+, 200 mg, 3 mL cartridge, Biotage, Sweden) at ambient sample pH. Between 500 mL ($S = 0$) and 2 L ($S = 35$) of each sample was passed in-line through a 0.2 μm PVDF filter cartridge (Sterivex, Sartorius) and then over the preconditioned cartridge (5 mL methanol, Optima LCMS grade, Fisher Scientific), 5 mL 0.1 mol L⁻¹ HCl (Trace metal grade, Fisher Scientific). The flow rate (ca. 10 mL min⁻¹) was regulated via a vacuum pump. All plastic that came into contact with the sample (polytetrafluoroethylene, polystyrene or high-density polyethylene) was acid washed (0.1 mol L⁻¹ HCl) prior to first use, and subsequently rinsed with ultrapure water. After preconcentration, excess seawater was removed from the cartridges, and the cartridges frozen at -20 °C and stored prior to extraction and analysis as described in the

Supplemental Information.

The concentration of dissolved organic carbon in the extracts (SPE-DOC) was determined after evaporation of a 200 μL sample aliquot to dryness in an oven (60 °C, 4

hours) in pre-combusted glass vials (450 °C, 8 hours). Residual carbon was re-dissolved in 0.1 mol L⁻¹ HCl and analyzed by high temperature catalytic oxidation using a TOC analyzer (Shimadzu) following the method described in Badr et al. 2003. Our blank values, obtained from evaporating 200 µL aliquots of the elution solution along with our samples, were subtracted from our determined DOC concentrations prior to correcting for preconcentration factors and calculation of the final SPE-DOC concentrations. We obtained a blank value of 1.37±0.2 µmol C L⁻¹ (*n* = 5).

3. Results

3.1. Sample grouping

Samples were grouped for analysis based on salinity and source (**Fig. 1**). Our study took place on the Northwest Brazilian Continental shelf in a region that included the outflow of the Amazon and Pará River estuaries, their northward flowing waters combined as the Amazon River Plume, a mangrove-influenced area to the southeast and the surrounding waters of the North Brazil Current (NBC). The “Amazon Transect” encompassed the Amazon River outflow region at a wide range of salinities (*S* ~0.3 - 35). To the south, the “Pará Transect” represented a distinct river catchment area (*S* ~0.4 - 28) fed by the Pará River and its main tributary the Tocantins River to the south. Upon estuarine mixing, the waters from both source rivers converge to form a plume of intermediate salinity (*S* ~ 10 - 26) that ages as it flows north (hereby referred to as “Plume North”). To the southeast of the Pará River, mangrove forests are a source of nutrients and organic matter from groundwater exchange (Dittmar and Lara 2001).

Samples collected parallel to this region (referred to as the “Mangrove Belt”) had salinities of 28 - 35 and elevated DOC concentrations (**Fig. 2b, 3b**). Finally, the NBC, which flows northwest from the South Equatorial current along the coast of northern Brazil, defined the seawater end members ($S \geq 35$).

3.2. Concentrations of chlorophyll *a*, dissolved organic carbon, silicate, nitrate and phosphate

Chl *a* concentration, a proxy for biomass, was highest in the mid-high salinity region, reaching a maximum of $28 \mu\text{g L}^{-1}$ ($S = 26.7$; **Fig. 2a, Fig. 3a**). On the other hand, DOC concentrations generally decreased with increasing salinity (**Fig. 2b, Fig. 3b**), ranging from $305 \mu\text{mol L}^{-1}$ ($S < 1$) to $40 \mu\text{mol L}^{-1}$ ($S > 35$), consistent with a large terrestrial input of DOM from both Amazon and Pará Rivers. In addition, elevated DOC concentrations were observed in the Mangrove Belt samples ($S > 28$).

Silicate, which derives from continental weathering and can serve as a riverine input tracer, also decreased as salinity increased (**Fig. 2c, Fig. 3c**). However, silicate drawdown was also observed in a few samples of intermediate salinity, indicating possible biological uptake (**Fig. 3c**). Nitrate concentrations decreased with increasing salinity but also showed a deviation below values expected from conservative mixing in the Amazon and Pará Transects in the mid salinity range ($S \sim 10 - 20$) (**Fig. 3d**). On the other hand, phosphate concentrations displayed a mid-salinity maximum (**Fig. 3e**). Nitrate-to-phosphate (N:P) ratios were highest in the river end member ($35 \mu\text{mol } \mu\text{mol}^{-1}$, **Supplemental table S2**), but decreased to $14 \mu\text{mol } \mu\text{mol}^{-1}$ at the phosphate maximum,

indicating that the increase in phosphate was likely the result of phosphate desorption and remobilization from sediments or suspended particles, rather than regeneration of organic matter.

3.3. Dissolved and soluble Cu distribution

Dissolved ($<0.2 \mu\text{m}$) and soluble ($<0.015 \mu\text{m}$) Cu concentrations both had a strong inverse correlation to salinity ($R = 0.95$ and 0.91 , respectively, $n = 102$ and 72 , respectively; $p < 0.0001$) (**Fig. 2d, Fig. 4a-b**), indicating that both size fractions were primarily governed by conservative mixing. Concentrations of dissolved Cu decreased from $35 \pm 3 \text{ nmol L}^{-1}$ in the Amazon River end member ($S = 0.3$) and $18 \pm 2 \text{ nmol L}^{-1}$ in the Pará River end member ($S = 0.4$) samples to $0.6 - 2.3 \text{ nmol L}^{-1}$ in the high-salinity NBC samples ($S \geq 35$) (**Fig. 4a**). Concentrations of soluble Cu followed a similar trend to the dissolved fraction and ranged from $25 \pm 3 \text{ nmol L}^{-1}$ ($S = 0.6$, Amazon Transect) and $14 \pm 3 \text{ nmol L}^{-1}$ ($S = 0.4$, Pará Transect) to $1.1 \pm 0.1 \text{ nmol L}^{-1}$ ($S = 35.8$) (**Fig. 4b**). Although Cu concentrations in the dissolved and soluble fractions correlated positively with each other (**Supplemental Fig. S1a,d, Supplemental Table S3**), local differences were apparent. A paired t-test showed that the data sets for soluble and dissolved Cu (**Supplemental Fig. S2a, Supplemental Table S4**) were significantly different from each other at low salinities ($S < 10$; $p = < 0.0001$, $n = 21$) but not overall ($S = 0.3-36$; $p > 0.05$, $n = 71$). The maximum large colloidal Cu concentration, defined as the difference between soluble ($<0.015 \mu\text{m}$) and dissolved ($<0.2 \mu\text{m}$) Cu, was observed in the Amazon River end member ($S = 0.3$, $15 \pm 5 \text{ nmol L}^{-1}$, 42% of dissolved) (**Fig. 4a-b, Fig. S2a, Supplemental**

Table S4). Our data therefore indicate that a low-salinity large colloidal Cu fraction exists, but decreases upon seawater mixing and subsequent flocculation.

For the ultrafiltered (UF) <1 and <10 kDa samples, Cu was analyzed from the L_{Cu} sample aliquots, since no UF samples were collected separately for Cu concentration analysis. Cu concentrations in the <10 kDa size fraction correlated positively with the dissolved and soluble fractions but had no significant correlation in the <1 kDa fraction (**Supplemental Fig. S1a,d, Supplemental Table S3**). In both the <1 and <10 kDa fractions, Cu concentrations decreased with respect to salinity, but generally increased when expressed as percentage of total Cu (**Fig. 4c**).

3.4. Apparent Cu-binding organic ligands, conditional stability constants and Cu^{2+} concentrations

In both dissolved and soluble size fractions, a single class of L_{Cu} ($12.6 \leq \log K'^{cond}_{CuL,Cu^{2+}} \leq 15.2$) (**Fig. 5a-b**) was detected in excess of Cu (**Fig. 4a**). We were unable to fit ~20% of the samples due to insufficient curvature (mostly the dissolved fraction in the low-salinity Amazon Transect; **Supplemental Table S1**), indicating that the detection window was too high for these samples or that strong binding sites were already saturated with Cu or other metals. In contrast to dissolved Cu (**Fig. 4a**) and DOC (**Fig. 3b**), concentrations dissolved L_{Cu} initially increased with respect to salinity (**Fig. 5a**), reaching a maximum of 83 ± 14 nmol eq Cu L^{-1} ($S = 6.2$) in the Amazon Transect and 76 ± 8 nmol eq Cu L^{-1} ($S = 9.8$) in the Plume North. The maxima were followed by a decrease in all samples as salinity increased.

L_{Cu} in the soluble fraction decreased with respect to salinity throughout the full salinity range (**Fig. 5b**) and correlated positively with the dissolved fraction (**Supplemental Fig. S1b,e, Supplemental Table S3**). Unlike the dissolved fraction however, no mid-salinity increase in soluble L_{Cu} was observed. As a result, the highest large colloid concentrations were observed from $S = 6.2$ (35 ± 15 nmol eq Cu L^{-1} , 43% of total) to $S = 9.8$ (57 ± 8 nmol eq Cu L^{-1} , 75% of total) (**Supplemental Fig. S2b, S3a, Supplemental Table S1.**).

Stability constants for Cu-organic ligand complexes ($\log K'^{cond}_{CuL,Cu2+}$) were generally lowest in low-mid salinity samples. In the dissolved fraction, the weakest ligands were detected at $S = 6.2$ in the Amazon Transect ($\log K'^{cond}_{CuL,Cu2+} = 12.6 \pm 0.1$) and at $S = 9.8$ in the Plume North ($\log K'^{cond}_{CuL,Cu2+} = 12.8 \pm 0.06$) (**Fig. 5c**), corresponding with the L_{Cu} concentration maxima (**Fig. 5a**). The strongest ligands in the dissolved size fraction were observed in the Pará River end member ($S = 0.4$, $\log K'^{cond}_{CuL,Cu2+} = 15.2 \pm 0.2$). For the other transects, the binding strength gradually increased with increasing salinity, reaching a maximum of $\log K'^{cond}_{CuL,Cu2+} = 14.5 \pm 0.1$ ($S = 34.2$). In the soluble size fraction, similar trends were observed (**Fig. 5d**). The apparently weakest ligands were present at $S = 5.6$ ($\log K'^{cond}_{CuL,Cu2+} = 13.2 \pm 0.05$), followed by an increase to a maximum at $S = 22.5$ ($\log K'^{cond}_{CuL,Cu2+} = 14.9 \pm 0.3$). For higher salinities, the stability constants remained relatively stable ($\log K'^{cond}_{CuL,Cu2+} = 14.2$ to 14.4).

The ultrafiltered (UF) L_{Cu} samples were lower in concentration than the soluble size fractions at the two lower salinities ($S = 0.3$, 19.1) and within error of the soluble size fraction at higher salinities ($S = 29.0$, 35.8) (**Fig. 5b**). In both UF fractions, L_{Cu}

concentrations decreased with respect to salinity (**Fig. 5b**), but only the <1 kDa showed a significant correlation with the dissolved and soluble fractions (**Supplemental Fig. S1b,e, Supplemental Table S3**). The stability constants for all ultrafiltered samples were uniformly high ($\log K'_{CuL,Cu2+}^{cond} = 14.9 \pm 0.4$ to 15.6 ± 0.2) (**Fig. 5d**) and generally exceeded those of the soluble and dissolved fractions (**Fig. 5c-d**).

To determine ligands present in excess of Cu (L_{Cu}'), the difference was taken between L_{Cu} and Cu concentrations measured in the speciation samples. In all dissolved samples where L_{Cu} could be calculated, ligands were present in excess of Cu (**Supplemental Fig. S3a-b**). The dissolved L_{Cu}' maxima were detected at $S = 6.1$ (60 ± 14 nmol eq Cu L^{-1}) and $S = 9.8$ (59 ± 8 nmol eq Cu L^{-1}) corresponding to maxima in total L_{Cu} (**Fig. 5a**). In the soluble fraction, L_{Cu}' also followed a similar trend to total soluble L_{Cu} concentrations (**Fig. 5b, f**) and decreased with respect to salinity.

Free Cu can be expressed as $pCu = -\log(Cu^{2+})$, where Cu^{2+} is the free Cu in mol L^{-1} . Free Cu was lowest in the dissolved Pará River end member sample ($pCu = 15 \pm 1$), which corresponded with a high $\log K'_{CuL,Cu2+}^{cond}$ (15.2 ± 0.1). The soluble and UF samples generally fell within the same range as the dissolved samples ($pCu \sim 13-16$, **Fig. 5f**), with two exceptions: the $S = 8.6$ soluble sample ($pCu = 10.1 \pm 0.3$) and the $S = 28.8$ <10 kDa UF sample ($pCu = 10.5 \pm 0.5$). In both cases, Cu concentrations apparently exceeded L_{Cu} (**Supplemental Table S1**).

α_{LCu} , is defined as the product of L_{Cu}' and $K'_{CuL,Cu2+}^{cond}$ (**Supplemental Fig. S3c-d**). In general, $\log \alpha_{LCu}$ followed a similar trend to pCu , as Cu^{2+} availability decreased with increased L_{Cu}' and $K'_{CuL,Cu2+}^{cond}$. We observed similar values among the soluble and

dissolved fractions ($\log \alpha_{\text{LCu}} \sim 5 - 7$). In general, the UF fractions were slightly higher than the corresponding dissolved and soluble samples, reflecting the high conditional stability constants.

3.5. Electroactive humic substances

In all samples, eHS (expressed in terms of Suwannee River Humic Acid, SRHA, as mg eq SRHA L⁻¹) were detected and predominated in the soluble size fraction (**Fig. 6a-b**), with large colloids present throughout a broad salinity range (**Supplemental Fig. S2c, Fig. S4c-d**). As observed for both Cu (**Fig. 4a-b**) and L_{Cu} (**Fig. 5a-b**), eHS generally decreased with respect to salinity (**Fig. 6a-b**), indicating a freshwater/terrestrial source. However, non-conservative behavior was also apparent, including a low-mid salinity maximum for dissolved samples similar to that observed for L_{Cu}. A maximum in concentration was observed in the Pará samples at $S = 5.1$ ($\text{eHS} = 3.8 \pm 0.3 \text{ mg eq SRHA L}^{-1}$) and similarly for the Amazon samples at $S = 8.2$ ($7.2 \pm 0.6 \text{ mg eq SRHA L}^{-1}$), although the latter was within error of the $S = 0.3$ Amazon River end member. In addition, the source of the river end member was important at low salinities: the Pará River end member ($S = 0.4$, $\text{eHS} = 2.5 \pm 0.3 \text{ mg eq SRHA L}^{-1}$) was much lower than the Amazon River end member ($S = 0.3$, $\text{eHS} = 6.3 \pm 0.7 \text{ mg eq SRHA L}^{-1}$). At higher salinities, eHS generally decreased until reaching a low $0.15 \pm 0.02 \text{ mg eq SRHA L}^{-1}$ ($S = 36.3$).

Soluble eHS concentrations also decreased with salinity but had a maximum concentration in the Amazon River transect at $S = 0.6$ ($\text{eHS} = 6.2 \pm 0.5 \text{ mg eq SRHA L}^{-1}$) (**Fig. 6b**). No soluble eHS data exist for the Pará Transect. As a result of the offset in

maxima between the soluble and dissolved fractions, a maximum in large colloids was observed at $S = 8.2$ (4.0 ± 0.6 mg eq SRHA L^{-1} , 55% of total). This follows a similar trend to the L_{Cu} large colloid fraction (maximum at $S = 6.2-9.8$), although large eHS colloids were detected throughout a broad salinity range (**Supplemental Fig. S2c, Supplemental Fig. S4b, Supplemental Table S5**).

3.6. Solid phase extractable Cu

Example SECs for UV absorbance at 254 nm (a_{254}) and Cu for four samples from the Amazon plume, Mangrove area and NBC are shown in the supplementary information (**Supplemental Fig. S5**). We observed two a_{254} nm peaks (**Supplemental Fig. S5**): a major, well-retained peak ($RT = 24.7 \pm 0.5$) that corresponded to a low molecular weight (LMW) fraction and a minor peak that was less well retained ($RT = 10.9 \pm 0.9$ min) and corresponded to a high molecular weight fraction. The LMW peak eluted at a similar retention time to our lowest PSS standard (4300 Da, $RT = 24.7$ min) but later than Suwanee River humic and fulvic acid ($RT: 22.13 \pm 0.09$ and 22.19 ± 0.07 mins respectively) and earlier than the peak for the vitamin thiamine (MW = 265, $RT = 27.6$). The HMW peak eluted earlier than our largest PSS standard (>150000 Da PSS equivalents). We observed only one well-retained peak for Cu in all samples (**Supplemental Fig. S5**) that largely co-eluted with the a_{254} nm peak, although the apex of the peak was typically slightly earlier (**Supplemental Fig. S5**, $RT = 24.3 \pm 0.3$).

Both SPE-Cu and a_{254} nm associated with the well retained peak correlated negatively with respect to salinity and followed a distribution expected from

conservative mixing (**Fig. 7a, Supplemental Table S6**). The maximum dissolved SPE-Cu (2.3 nmol L⁻¹) was observed in the Amazon River end member sample ($S = 0.03$). Concentrations declined to ≤ 0.02 nmol L⁻¹ in the offshore NBC seawater end member samples ($S > 35$). Concentrations of SPE-Cu strongly correlated with the LMW a254 peak areas ($R = 0.99$, $n = 24$, $p < 0.001$). Interestingly, the Mangrove Belt stations were elevated in SPE-Cu relative to the Amazon, Pará and NBC stations in a similar salinity range (**Fig. 7a, Supplemental Table S6**), which was also reflected in several DOC data points (**Fig. 3b**).

Comparison of SPE-DOC with DOC concentrations determined in samples collected at the same depth and stations resulted in linear relationship ($R^2 = 0.44$, $p < 0.01$, $n = 22$) with an intercept within error of zero (-0.2 ± 2.9) (**Supplemental Fig. S6, Supplemental Table S7**). The slope (0.08 ± 0.02) suggested a relatively low recovery of 8% compared to recoveries typically obtained for preconcentration of DOC at pH 2 using PPL resins (e.g. 40 to 75 %; (Green et al. 2014 and references therein), but similar to efficiencies (ca. 10%) previously observed for neutral extractions of DOC from coastal seawater (Waska et al. 2015).

Samples for dissolved Cu analysis were collected from the towed-fish whilst underway, whereas samples for SPE-Cu were collected on station using the standard CTD, therefore the recovery for Cu was estimated using the slopes of their respective salinity-plots. A negative linear relationship with respect to salinity was observed for both dissolved Cu (slope = -0.60 ± 0.02 , $R = 0.95$, $n = 102$, $p < 0.0001$) and SPE-Cu (slope = -0.039 ± 0.004 , $R = 0.88$, $n = 24$, $p < 0.0001$), yielding a Cu recovery of $7 \pm 1\%$.

4. Discussion

4.1. Cu in the Amazon remains largely conservative and below potentially toxic levels

Dissolved Cu distributions largely followed values expected from conservative mixing, although we observed differences between estuarine regions, reflecting different freshwater and terrestrial sources (Amazon River, Pará River and Mangrove Belt). Linear regression of dissolved Cu concentrations vs. salinity (nmol L^{-1} Cu per unit salinity; **Table 2**) showed the steepest Cu decline in the Amazon Transect, followed by the Plume North, the Pará Transect and the Mangrove Belt. The NBC stations ($S \geq 35$) did not have a significant linear relationship with salinity ($p > 0.05$). The slopes of the Amazon, Plume North and Pará Transects were lower in the soluble than in the dissolved fraction, reflecting an early decrease in large Cu-bearing colloids.

Growth inhibition due to Cu toxicity may occur for eukaryotic phytoplankton at $p\text{Cu} < 12$ ($\text{Cu}^{2+} > 10 \text{ pM}$), and for cyanobacteria at $p\text{Cu} < 13$ ($> 1 \text{ pM}$) (Brand et al. 1986). In all dissolved samples, free Cu remained below potentially toxic concentrations ($p\text{Cu} > 13$), although in one soluble and one UF sample, $p\text{Cu}$ was below 13 (**Fig. 5d-e**). In the environment however, all size fractions of ligands exist together and can exchange ions (Dulaquais et al. 2020). Thus, our dissolved $p\text{Cu}$ data indicate that Cu^{2+} did not likely reach levels potentially toxic to phytoplankton.

The mostly conservative behavior of Cu across the salinity gradient is consistent with previous estuarine studies in a variety of different environments: similar trends have been observed in the Amazon River estuary in a previous study (Boyle et al. 1982),

the Bang Pakong River estuary in Thailand (Windom et al. 1988), the Po River plume in the Adriatic (Illuminati et al. 2019), several North American estuaries (Cutter 1991) and several Chinese river systems including the Yangtze, Minjiang and Jiulongjiang River estuaries (Zhang 1995). On the other hand, deviations from conservative behavior have also been reported in some estuaries, and may result from Cu-removal to scavenging, colloidal flocculation and/or biological uptake (Windom et al. 1988; Abdel-Moati 1990; Zhang 1995; Tang et al. 2002; Pavoni et al. 2020). Despite observed biological productivity however, evidenced by elevated Chl *a* concentrations (Figure 3a) and silicate drawdown (Figure 3c) attributed to diatom growth (Zhang et al. 2020), we observed a mostly conservative distribution of Cu in the study area.

A comprehensive study of major Amazon tributaries quantified the overall trace metal fluxes from the Amazon River, and observed increased Cu concentrations during higher seasonal discharge conditions (Seyler and Boaventura 2003); however, the study evaluated only riverine samples, and the authors called for a need for further estuary studies due to the complicating factors involved in river-seawater mixing. Boyle et al. (1982) observed a Cu distribution governed mostly by conservative mixing in the Amazon estuary and mixing plume on two cruises in June of 1974 and 1976 (**Fig. 8**), with non-conservative Cu drawdown corresponding to an unusually slow circulating plume in 1974. In more recent decades however, the Amazon catchment area has experienced major anthropogenic disturbances (Coe et al. 2009; Davidson et al. 2012; Castello et al. 2013), which can be expected to have an impact on trace metals in the Amazon River. For example, forest fires in the Amazon emit large amounts of Mn, Cu and Zn into the

atmosphere (Yamasoe et al. 2000) and gold mining can cause Hg, Cu and Zn pollution in sediments and soils (Rodrigues Filho and Maddock 1997; Lacerda et al. 2004; Cesar et al. 2011). Despite these anthropogenic impacts to the Amazon basin, our study finds remarkably little change compared to 1976 (Boyle et al. 1982) for dissolved Cu concentration in the Amazon River estuary region and mixing plume during the high-discharge period (**Fig. 8**).

4.2. Soluble ligands mitigate large colloidal Cu formation

Deviations from conservative mixing behavior of Cu and other metals has been attributed to colloidal flocculation upon river-seawater mixing in a variety of different estuaries (Sholkovitz 1976; Abdel-Moati 1990; Zhang 1995; Tang et al. 2001; Pearson et al. 2017; Pavoni et al. 2020). In contrast, we observed mostly conservative behavior in Cu concentrations in the dissolved and soluble fraction (**Fig. 4, Supplemental Fig. S2a**). Our data therefore show that Cu concentrations in the study area are influenced primarily by physical mixing, although a minor large-colloid fraction at low salinity ($S < 10$) also suggest that dissolved Cu is partly influenced by colloidal flocculation during early mixing.

On the other hand, we detected distinct low-mid salinity maxima for large L_{Cu} colloids ($S = 9.8$, $57 \pm 8 \text{ nmol L}^{-1}$, 75% of total) and eHS ($S = 8.2$, $4.0 \pm 0.6 \text{ mg eq SRHA L}^{-1}$, 55% of total) (**Supplemental Fig. S2b-c, Supplemental Fig. S4**). Our L_{Cu} and eHS data are similar to a recent study in the Loire River estuary (France), which observed a positive anomaly in the dissolved fractions of at $S \sim 4.5$, while the soluble fractions were more

conservative (Dulaquais et al. 2020). Our results suggest that the strong buffering of Cu by organic ligands mitigates formation of large Cu-containing colloids, and subsequent colloidal flocculation, throughout most of the estuary. It is also worth noting however, that competition with other metals such as iron (Fe) may also play a role in excluding Cu from the colloidal phase. Competition for ligands among trace metals depends on both the concentrations of these trace metals and the character of binding sites in the ligands present (Avendaño et al. 2016), and high concentrations of Fe(III) bound to organic matter and colloidal Fe-oxides can inhibit the formation of colloidal Cu-humic substance complexes when the ratio of dissolved Fe to Cu is high (Muller and Cuscov 2017). Future studies into Fe and Fe-binding ligands in this region are needed for a more complete understanding of the role of trace metal-organic ligand competition in the Amazon estuary.

The conditional stability constants ($\log K'_{CuL,Cu2+}^{cond}$ 12.6 - 15.2) of the Cu-complexing ligands were similar across all size fractions, and comparable to values reported previously in other estuaries ($\log K'_{CuL,Cu2+}^{cond}$ range ~11-16; Tang et al. 2001; Shank et al. 2004; Muller and Batchelli 2013; Whitby et al. 2017; Dulaquais et al. 2020). In general, we observed slightly higher $\log K'_{CuL,Cu2+}^{cond}$ in the soluble fraction than the dissolved size fractions, and highest values in the UF (<1 kDa and <10 kDa) fractions (**Fig. 5c-d**). The apparently weaker large colloidal fraction is consistent with the observed preferential size partitioning of Cu into the soluble fraction, which is buffered by comparatively stronger ligands. Similar trends in relative binding strength (stronger smaller ligands and weaker larger ligands) were observed in previous estuarine studies

(Wells et al. 1998; Muller and Batchelli 2013), although other studies have observed opposite trends (Tang et al. 2001; Dulaquais et al. 2020), or no significant association between size fractionation and binding strength (Muller and Cuscov 2017).

The lowest $\log K'_{CuL,Cu2+}^{cond}$ was detected at the dissolved and large colloidal L_{Cu} maximum (**Fig. 5c**). The observed increase in weaker L_{Cu} as well as eHS may suggest a possible source of autochthonous ligand production in addition to the terrestrially-derived pool (Muller and Batchelli 2013). Cu-binding ligands and humic-like substances can be produced during phytoplankton growth (Lorenzo et al. 2007; Mellett et al. 2018; Nixon et al. 2019) or decay (Lorenzo et al. 2007), and we observed primary production (Chl *a* production, macronutrient drawdown; **Fig. 3**) across a wide salinity range. This is consistent with input of phytoplankton-derived DOM in regions of the plume where turbidity decreases due to flocculation of riverine particles, although terrestrial DOM generally remains dominant in the river plume (Medeiros et al. 2015).

Ultrafiltered (UF) concentrations of Cu (**Fig. 4c**) and L_{Cu} (**Fig. 5b**) were either lower than or within error of the soluble fractions in all samples. The <1 and <10 kDa fractions are defined by weight, and therefore do not have a direct relationship to pore size, but weight and pore size have been empirically related for different filter membranes. For Millipore membranes, a weight range of 1 - 10 kDa has been found to correspond an estimated pore diameter range of ~2.8 - 4.4 nm (Sarbolouki 1982), well below the 0.015 μm maximum for the soluble size fraction. While the concentration of <1 and <10 kDa Cu decreased with increasing salinity, it increased as a percentage of total dissolved Cu, with <1 kDa Cu increasing from $9 \pm 1\%$ in the Amazon River end

member to $75 \pm 8\%$ in the NBC seawater end member. Similarly, <1 and <10 kDa L_{Cu} were much lower in concentration than the soluble fraction in the riverine end member, but indistinguishable from the soluble fraction at higher salinities. This suggests that Cu and L_{Cu} were associated with a distinct class of smaller colloids (4.4 to 15 nm) present mainly at low salinities.

The inverse correlation between measured $\log K'_{CuL,Cu2+}^{cond}$ and L_{Cu} concentrations (**Supplemental Fig. S7**) in both the dissolved ($R = 0.7$, $n = 16$, $p < 0.01$) and soluble ($R = 0.6$, $n = 20$, $p < 0.01$, $n = 20$) fractions may be partly a reflection of Cu concentrations, as higher Cu can be expected to both decrease apparent binding strength and increase apparent L_{Cu} . This correlation indicates a ligand pool with a highly heterogeneous mixture of binding sites (Town and Filella 2000b), and the measured L_{Cu} reflects an average across different binding strengths.

We further characterized the relative molecular size of a hydrophobic Cu and DOC pool isolated by SPE at neutral pH via HPSEC. As expected from our Cu and DOC concentration data (**Fig. 3b**, **Fig. 4a**) and a previous study of estuarine SPE metals and DOM (Ksionzek et al. 2018), SPE-Cu decreased with increasing salinity. We extracted an estimated $7 \pm 1\%$ of the dissolved Cu pool and $8 \pm 2\%$ of the DOC at neutral pH, and the relatively low recovery for DOC of the neutral SPE extractions could thus explain the relatively low SPE-Cu concentration values compared to dissolved Cu (**Fig. 4a**). All of the Cu in this fraction eluted within the size range between thiamine and Suwannee River humic and fulvic acids and is thus comparable in size to the <10 kDa ultrafiltered fraction. Furthermore, the size range of our isolated DOM is similar to size ranges

previously determined for natural organic matter isolated from aquatic environments by solid phase extraction (Perminova et al. 2003). The Cu peak coeluted with the broad a254 absorbance peak. A detailed discussion of the spectrophotometric and spectrometric character of this broad peak will be presented elsewhere, however we note that the broad a254 nm peaks obtained for our estuarine samples are consistent with previous studies of size exclusion chromatography of natural organic matter (Perminova et al. 2003; Woods et al. 2010; Hawkes et al. 2019). Such broad peaks are considered to comprise a heterogeneous mixture of organic compounds that incorporate aromatic compounds, carboxylic-rich alicyclic molecules (CRAM) and small biomolecules (Hawkes et al., 2019, Wood et al., 2009). The coelution of Cu with this peak therefore supports a strong link between Cu and the bulk components of DOM in the study area and suggests that at least 8% of the dissolved Cu pool is complexed to binding sites within DOM that are heterogeneous in character. This is thus consistent with our eHS results and the heterogeneity suggested by the inverse correlation between $\log K'^{cond}_{CuL,Cu2+}$ and L_{Cu} (**Supplemental Fig. S7**).

Taken together, our results suggest that riverine DOM is the primary control on Cu transport and speciation in this part of the Northwest Brazilian Continental Shelf. In contrast to eHS and apparent L_{Cu} , no increase in SPE-Cu was observed in the low to mid-salinity range. As SPE is known to also fractionate natural organic matter according to size (Raeke et al. 2016; Hawkes et al. 2019), we note that it is possible that the SPE method we used does not preconcentrate this colloidal fraction. Nevertheless, our SPE-

Cu data mirrors the Cu concentrations and is consistent with the partitioning of dissolved Cu primarily into the soluble fraction.

4.3. Distinct source signatures are observed from the Amazon and Pará Rivers and Mangrove Belt

Differences were noted between the Pará and Amazon River outflow regions. Dissolved and soluble Cu concentrations (**Fig. 4a-b**) and dissolved eHS (**Fig. 6a**) were much higher in the Amazon River end member samples. Interestingly, the dissolved Pará River end member also had the highest $\log K'^{cond}_{CuL,Cu2+}$ of all the dissolved samples measured (**Fig. 5c**). These apparently strong Pará ligands corresponded to a higher pCu (**Fig. 5e**), although all dissolved samples remained below potentially toxic levels of free Cu ($pCu \geq 13$). These findings highlight differences in the concentrations of dissolved and free Cu, as well as different compositions of organic ligands, eHS and their binding strength in the Amazon and Pará River outflow regions. However, these differences equalized quickly upon estuarine mixing ($S \geq 10$), and the Amazon, Pará and Plume North transects follow a similar trend at higher salinities.

The differences between the Amazon and Pará Rivers may be partly attributed to their distinct catchment areas. The Pará River is fed from the Tocantins River and watershed to the south, which has suffered greater anthropogenic impacts from deforestation and agricultural development (Coe et al. 2009). As a result, the Tocantins has experienced increased surface runoff and volume output over the past ~70 years

(Costa et al. 2003), which can be expected to alter its geochemistry and trace metal concentrations.

During sampling, a noticeable green coloration in the water at the Mangrove Belt was observed and attributed to an influx of mangrove-derived groundwater and heightened productivity. Mangroves contribute more than 10% of the refractory terrestrial DOC to the global oceans (Dittmar et al. 2006). Indeed, several of the Mangrove Belt samples ($S \sim 29 - 32$) displayed elevated DOC concentrations and SPE-Cu (**Fig. 3b, Fig. 7a**) compared to values expected from purely conservative mixing, although this was not observed for eHS or L_{Cu} (**Fig. 5-6**). A distinct fraction of small colloidal Cu (1 kDa-10 kDa) was also observed in the Mangrove Belt ($S = 28.8$, **Fig. 4c**), but was not detected in the NBC ($S = 35.8$) or mid-salinity Amazon ($S = 19.1$) samples. These apparent anomalies in the Mangrove Belt may be partly attributed to the influence of macrotides that flood the mangrove forests (Lara and Dittmar 1999), leading to an influx of nutrient- and DOM-rich groundwater (Dittmar and Lara 2001).

4.4. Comparison of analyses

Three approaches discussed in this paper (voltammetric determination of L_{Cu} and binding strength using SA, voltammetric determination of eHS using SRHA, and determination of SPE-Cu with SEC) provide complimentary ways to analyze different aspects of Cu-organic matter speciation. Our data confirm the importance of organic complexation, primarily with terrestrial organic ligands, in governing the behavior of Cu and preventing free Cu from reaching potentially toxic levels in the Amazon and Pará

River estuaries, Mangrove Belt and mixing plume. While Cu binding sites were detected in both soluble and dissolved fractions, Cu appears to be preferentially partitioned into the soluble fraction, although a minor large-colloidal Cu fraction was also detected at low salinity. The apparent solubilization of Cu is consistent with the high affinity of Cu for DOM and low affinity to particles.

Despite the good agreement among the methods utilized, each has advantages and limitations. Voltammetric ligand analysis, while instructive, is necessarily an oversimplification in heterogeneous solutions. The traditional fitting to one or two ligand classes cannot fully measure the heterogeneity that is actually present in organic matter, and which results in a distribution of stability constant values (Town and Filella 2000a; Town and Filella 2000b). We were only able to achieve single-ligand class fitting in most samples, although the observed inverse correlation between apparent L_{Cu} and $\log K'_{CuL,Cu2+}^{cond}$ indicate a high degree of heterogeneity (**Supplemental Fig. S7**). In reality, the calculated values for $\log K'_{CuL,Cu2+}^{cond}$ are conditional averages, and the two parameters are not truly independent, so that an increase in L_{Cu} will be reflected by a decrease in $\log K'_{CuL,Cu2+}^{cond}$. Furthermore, our values for L_{Cu} and $\log K'_{CuL,Cu2+}^{cond}$ were both more variable than eHS and SPE-Cu, indicating that the results may be partly influenced by the variable ionic strength of the estuarine samples or variable Cu concentrations. One way to better represent the wide distribution of ligands is to use more than one detection window (Town and Filella 2000b; Buck and Bruland 2005), but due to limited sample volume, we could only apply a single detection window, and so the scope of detectable L_{Cu} concentrations and conditional stability constants was limited. In

addition, we were unable to calculate L_{Cu} and $\log K'_{CuL,Cu2+}^{cond}$ in 12 out of 59 samples
(**Table S1**) due to insufficient curvature in the titrations, indicating that the detection
window may have been too high, or that binding sites were already saturated with Cu or
other metals. Future analysis at multiple detection windows would likely provide an
improved picture of the full range of Cu-organic matter interaction in this region.

Measuring eHS in terms of SRHA enabled us to quantify the humic-like portion of
the ligand pool. However, as humic substances represent a range of molecular weights
and binding capacities, any conversion to moles is necessarily an estimate. Such
conversions have been made in other studies using titrations with Suwannee River
humic and fulvic acid standards (Dulaquais et al. 2020; Whitby and van den Berg 2015).
The Amazon River plume contains a large fraction of terrestrial DOM but additional
autochthonous DOM is added in the plume by phytoplankton and terrestrial DOM is
continuously altered by bacterial and photochemical transformations (Medeiros et al.,
2015). This complex DOM mixture is rather different from the Suwannee River
standards, including suspected autochthonous ligand production in the plume, and
therefore it was not possible to establish quantitative binding capacities for eHS
throughout the entire river-to-ocean-continuum. Nevertheless, initial estimates based
on the relationship of eHS to dissolved Cu suggest a binding capacity of approximately
3.3 nmol L⁻¹ Cu per mg of eHS for the dissolved fraction and 4.0 nmol L⁻¹ Cu per mg eHS
for the soluble fraction (**Supplemental Fig. S8, Supplemental Table S8**), which are in
good agreement with previously reported values (Kogut and Voelker 2001). This value is
lower than values reported in some European estuaries (Whitby and van den Berg 2015;

Dulaquais et al. 2018). Using this estimate to compare the concentrations of eHS to dissolved Cu and Cu-binding ligand concentrations, eHS appear to compose a variable fraction of total L_{Cu} , with the lowest contribution at low salinities (**Supplemental Fig. S9, Supplemental Table S5**). This is consistent with findings by Dulaquais et al. (2020) and Whitby et al. (2017), where other Cu-specific groups such as thiols and amino acids dominate Cu complexation at low salinities. In the future, further method development will be useful to more rigorously quantify eHS binding strength and molar concentration specific to the study area, in order to better quantify eHS in the Amazon estuary.

Solid phase extraction provided a third approach to assess a portion of the Cu-organic pool by isolating and quantifying a selective hydrophobic Cu fraction. Due to low yield (ca 7%, see section 3.6), the reported SPE-Cu reflects a relatively small fraction of the total Cu-organic matter. Nevertheless, our SPE-Cu results showed similar trends compared to DOC, Cu and eHS (**Fig. 3a, Fig. 4a-b, Fig. 7a**). Furthermore, this method can be paired with mass spectrometry to characterize DOM at a molecular level (Waska et al. 2015). In future studies, this approach can be used to further understand the composition Cu-organic matter pool.

4.5 Limitations and future direction

All size classes are operationally-defined. Although our colloidal size range is similar to a previous estuarine study (Dulaquais et al. 2020), other studies use a range of lower cut-offs from 1 kDa to 10 kDa (e.g. Wilkinson et al. 1997; Wells et al. 1998; Tang et al. 2001; Muller and Batchelli 2013; Pavoni et al. 2020), making direct comparison of

these size fractions challenging. Moreover, the observed size partitioning may partly reflect biases during filtration. Although stringent trace metal protocols were followed, the higher-than-expected contribution of the soluble fraction (soluble > dissolved) at low concentrations indicates that some contamination may have occurred, as the soluble fraction requires an additional filtration step. It is also possible that changing ionic strength influenced apparent Cu and L_{Cu} concentrations by altering membrane and/or particle size. Higher ionic strength solutions may be expected to make the volume of a gel membrane shrink, possibly causing an underreporting of the <1 and <10 kDa size fractions. On the other hand, increased ionic strength and pH can shrink colloids by altering charge and enhancing electrostatic bonding, resulting in apparently higher concentrations at higher salinity, although this same mechanism can also increase colloidal aggregation (Mosley et al. 2003; Mosley and Liss 2020). The observed increased dominance of the smallest size fractions of Cu (**Fig. 4c**) and L_{Cu} (**Fig. 5b**) at higher salinities may therefore be partly related to particle size decrease at higher ionic strengths and higher pH. Although our <10 kDa Cu data were in good agreement with our SEC data, which isolated SPE-Cu based on weight, these possible biases cannot be ruled out.

In addition to influencing particle size and colloidal aggregation, changes in pH and ionic strength also influence trace metal-DOM binding. pH in estuaries is generally expected to decrease slightly at low salinities, followed by an increase and finally stabilization at higher salinities ($S > 15$) (Mosley and Liss 2020). Modeling has shown that increasing ionic strength will tend to decrease Cu-DOM complexation, as divalent

cations (such as Mg^{2+}) compete with Cu for DOM, and the displaced Cu can then bind to Fe oxi(hydroxi)des (Mosley and Liss 2020). Decreasing pH also decreases Cu-DOM interaction, as protons also compete with Cu for DOM, and $\log K'_{\text{CuL,Cu}^{2+}}^{\text{cond}}$ (Gledhill et al. 2015). Similarly, Cu-humic binding has been shown to decrease with increasing salinity and decreasing pH (Hamilton-Taylor et al. 2002). As marine and estuarine pH is subject to change as a result of anthropogenic impacts including increases in CO_2 , further investigation of the role of pH in Cu speciation in the study area is warranted.

Finally, the high seasonal fluctuation in Amazon River discharge (Villar et al. 2009) likely plays an important role in Cu-DOM cycling and warrants further study. In other estuaries, Cu concentrations and size-partitioning are known to be altered by seasonality and river discharge. For example, Windom et al. (1988) observed a non-conservative decrease in Cu at low salinities ($\sim S < 5$) during the high discharge season but not the low discharge season for the Bang Pankong estuary, which was attributed to possible particle scavenging to resuspended sediments or Fe-oxides. A recent study in the Isonzo River estuary (Italy) also observed a seasonal effect on size-partitioning, with depletion in the smallest size fraction (< 10 kDa) of Cu during the wet seasons (Pavoni et al. 2020). Similarly, a study in the River Thurso estuary (Scotland) observed decreased partitioning of Cu and L_{Cu} to the smallest (< 1 kDa) size fraction with increased river flow (Muller and Cuscov 2017). Given the likely importance of seasonality for trace metal cycling in the Amazon River plume, a follow-up study is planned during low-discharge conditions. The combination of low and high discharge data will enable us to quantify

the annual input of Cu into the Atlantic and to estimate the interannual variability of overall processes that influence this input.

5. Conclusions

Our study provides a novel assessment of the contribution of the Amazon and Pará Rivers as a source of Cu as a nutrient to the tropical North Atlantic Ocean, and the role of organic ligands in buffering potential Cu toxicity. Cu was primarily present in the soluble ($<0.015\ \mu\text{m}$) fraction, and concentrations were governed mostly by physical mixing. A heterogeneous pool of Cu-binding organic ligands was characterized by high conditional stability constants ($\log K'_{\text{CuL,Cu}^{2+}}^{\text{cond}} = 12.6\text{-}15.2$) was present in excess of ambient Cu concentrations. Humic substances (measured as eHS) followed a similar trend compared to L_{Cu} . As a result of the buffering effects of organic ligands, Cu^{2+} never reached levels potentially toxic for phytoplankton, indicating that the anthropogenic disruptions to the Amazon basin region have not yet caused Cu pollution of the coastal ocean.

Although Cu was found predominantly in the soluble fraction, a pool of large (0.015 to $0.2\ \mu\text{m}$) colloidal Cu was also detected at low salinities, indicating that colloidal formation and flocculation occurred during early mixing in the Amazon and Pará estuaries. On the other hand, we detected a broad mid-salinity fraction of large L_{Cu} and eHS colloids, suggesting a source of autochthonous (phytoplankton-derived) ligand production in addition to terrestrially-derived organic ligands. The soluble and ultrafiltered (where available) size fractions of eHS and L_{Cu} behaved more

conservatively, suggestive of a predominately terrestrial ligand source. SPE-Cu followed a similar conservative trend and was consistent with the results observed for the <10 kDa Cu fraction. Conditional stability constants ($K'_{CuL,Cu2+}^{cond}$) for L_{Cu} were higher in the soluble than in the dissolved fraction and highest in the ultrafiltered samples. Thus, the primarily conservative distribution of Cu concentrations and the dominance in the soluble fraction likely reflects stabilization of Cu by an abundance of strong soluble organic ligands.

Over the past several decades, the Amazon catchment area has been subject to strong anthropogenic changes, including deforestation, forest fires, hydropower dams and the consequences of climate change. Our comparison to previous data indicates that Cu concentrations are comparable to the 1970s, suggesting that, so far, the large overall river flow may compensate the impact of potential Cu pollution. Further studies to assess seasonal discharge variability between the dry and the rainy period will enable us to characterize the export of Cu and organic-Cu complexes from the Amazon River basin to the coastal ocean and, ultimately the contribution of Cu to the Atlantic Ocean via the Brazil current and meridional overturning circulation. Together, these studies will enable us to assess how future anthropogenic changes in this region will affect the export of Cu and Cu-associated organic matter, to the Atlantic Ocean.

References

- Abdel-Moati, A. R. 1990. Behaviour and fluxes of copper and lead in the Nile River estuary. *Estuar. Coast. Shelf Sci.* **30**: 153-165. [https://doi.org/10.1016/0272-7714\(90\)90061-U](https://doi.org/10.1016/0272-7714(90)90061-U)
- Annett, A. L., S. Lapi, T. J. Ruth, and M. T. Maldonado. 2008. The effects of Cu and Fe availability on the growth and Cu: C ratios of marine diatoms. *Limnol. Oceanogr.* **53**: 2451-2461. <https://doi.org/10.4319/lo.2008.53.6.2451>
- Aucour, A.-M., F.-X. Tao, P. Moreira-Turcq, P. Seyler, S. Sheppard, and M. F. Benedetti. 2003. The Amazon River: behaviour of metals (Fe, Al, Mn) and dissolved organic matter in the initial mixing at the Rio Negro/Solimões confluence. *Chem. Geol.* **197**: 271-285. [https://doi.org/10.1016/S0009-2541\(02\)00398-4](https://doi.org/10.1016/S0009-2541(02)00398-4)
- Avendaño, L., M. Gledhill, E. P. Achterberg, V. Rerolle, and C. Schlosser. 2016. Influence of ocean acidification on the organic complexation of iron and copper in Northwest European shelf seas; a combined observational and model study. *Front. Mar. Sci.* **3**. <https://doi.org/10.3389/fmars.2016.00058>
- Badr, E.-S. A., E. P. Achterberg, A. D. Tappin, S. J. Hill, and C. B. Braungardt. 2003. Determination of dissolved organic nitrogen in natural waters using high-temperature catalytic oxidation. *TRAC-Tend Anal. Chem.* **22**: 819-827. [https://doi.org/10.1016/S0165-9936\(03\)01202-0](https://doi.org/10.1016/S0165-9936(03)01202-0)
- Beck, A. J., J. K. Cochran, and S. A. Sañudo-Wilhelmy. 2010. The distribution and speciation of dissolved trace metals in a shallow subterranean estuary. *Mar. Chem.* **121**: 145-156. <https://doi.org/10.1016/j.marchem.2010.04.003>
- Boiteau, R. M., C. P. Till, A. Ruacho, *et al.* 2016. Structural characterization of natural nickel and copper binding ligands along the US GEOTRACES Eastern Pacific Zonal Transect. *Front. Mar. Sci.* **3**: 243. <https://doi.org/10.3389/fmars.2016.00243>

878 Boyle, E. A., S. S. Husted, and B. Grant. 1982. The chemical mass balance of the Amazon
879 Plume—II. Copper, nickel, and cadmium. *Deep Sea Res. Part I Oceanogr. Res. Papers* **29**:
880 1355-1364. [https://doi.org/10.1016/0198-0149\(82\)90013-9](https://doi.org/10.1016/0198-0149(82)90013-9)

881 Brand, L. E., W. G. Sunda, and R. R. L. Guillard. 1986. Reduction of marine phytoplankton
882 reproduction rates by copper and cadmium. *J Exp. Mar. Bio. Ecol.* **96**: 225-250.
883 [https://doi.org/10.1016/0022-0981\(86\)90205-4](https://doi.org/10.1016/0022-0981(86)90205-4)

884 Buck, K. N., and K. W. Bruland. 2005. Copper speciation in San Francisco Bay: a novel approach
885 using multiple analytical windows. *Mar. Chem.* **96**: 185-198.
886 <https://doi.org/10.1016/j.marchem.2005.01.001>

887 Bundy, R. M., K. A. Barbeau, and K. N. Buck. 2013. Sources of strong copper-binding ligands in
888 Antarctic Peninsula surface waters. *Deep Sea Res. Part II Top. Stud. Ocenogr.* **90**: 134-
889 146. <https://doi.org/10.1016/j.dsr2.2012.07.023>

890 Campos, M. L. A., and C. M. G. van den Berg. 1994. Determination of copper complexation in sea
891 water by cathodic stripping voltammetry and ligand competition with salicylaldoxime.
892 *Anal. Chim. Acta* **284**: 481-496. [https://doi.org/10.1016/0003-2670\(94\)85055-0](https://doi.org/10.1016/0003-2670(94)85055-0)

893 Castello, L., D. G. McGrath, L. L. Hess, *et al.* 2013. The vulnerability of Amazon freshwater
894 ecosystems. *Conserv. Lett.* **6**: 217-229. <https://doi.org/10.1111/conl.12008>

895 Cesar, R., S. Egler, H. Polivanov, Z. Castilhos, and A. P. Rodrigues. 2011. Mercury, copper and zinc
896 contamination in soils and fluvial sediments from an abandoned gold mining area in
897 southern Minas Gerais State, Brazil. *Environ. Earth Sci.* **64**: 211-222.
898 <https://doi.org/10.1007/s12665-010-0840-8>

899 Coale, K. H., and K. W. Bruland. 1988. Copper complexation in the Northeast Pacific. *Limnol.*
900 *Oceanogr.* **33**: 1084-1101. <https://doi.org/10.4319/lo.1988.33.5.1084>

901 Coe, M. T., M. H. Costa, and B. S. Soares-Filho. 2009. The influence of historical and potential
 902 future deforestation on the stream flow of the Amazon River—Land surface processes
 903 and atmospheric feedbacks. *J. Hydrol.* **369**: 165-174.
 904 <https://doi.org/10.1016/j.jhydrol.2009.02.043>

905 Costa, M. H., A. Botta, and J. A. Cardille. 2003. Effects of large-scale changes in land cover on the
 906 discharge of the Tocantins River, Southeastern Amazonia. *J. Hydrol.* **283**: 206-217.
 907 [https://doi.org/10.1016/S0022-1694\(03\)00267-1](https://doi.org/10.1016/S0022-1694(03)00267-1)

908 Cutter, G. A. 1991. Trace Elements in Estuarine and Coastal Waters-US Studies from 1986–1990.
 909 *Rev. Geophys.* **29**: 639-644. <https://doi.org/10.1002/rog.1991.29.s2.639>

910 Davidson, E. A., A. C. de Araújo, P. Artaxo, *et al.* 2012. The Amazon basin in transition. *Nature*
 911 **481**: 321. <https://doi.org/10.1038/nature10717>

912 de Abreu, C. H. M., M. d. L. C. Barros, D. C. Brito, M. R. Teixeira, and A. C. d. Cunha. 2020.
 913 Hydrodynamic modeling and simulation of water residence time in the Estuary of the
 914 Lower Amazon River. *Water* **12**: 660. <https://doi.org/10.3390/w12030660>

915 Dittmar, T., N. Hertkorn, G. Kattner, and R. J. Lara. 2006. Mangroves, a major source of dissolved
 916 organic carbon to the oceans. *Global Biogeochem. Cycles* **20**.
 917 <https://doi.org/10.1029/2005GB002570>

918 Dittmar, T., and R. J. Lara. 2001. Driving forces behind nutrient and organic matter dynamics in a
 919 mangrove tidal creek in North Brazil. *Estuar. Coast. Shelf Sci.* **52**: 249-259.
 920 <https://doi.org/10.1006/ecss.2000.0743>

921 Dryden, C. L., A. S. Gordon, and J. R. Donat. 2007. Seasonal survey of copper-complexing ligands
 922 and thiol compounds in a heavily utilized, urban estuary: Elizabeth River, Virginia. *Mar.*
 923 *Chem.* **103**: 276-288. <https://doi.org/10.1016/j.marchem.2006.09.003>

924 Dulaquais, G., M. Waeles, J. Breitenstein, J. Knoery, and R. Riso. 2020. Links between size
 925 fractionation, chemical speciation of dissolved copper and chemical speciation of
 926 dissolved organic matter in the Loire estuary. *Environ. Chem.*
 927 <https://doi.org/10.1071/EN19137>

928 Dulaquais, G., M. Waeles, L. J. A. Gerringa, R. Middag, M. J. A. Rijkenberg, and R. Riso. 2018. The
 929 biogeochemistry of electroactive humic substances and its connection to iron chemistry
 930 in the North East Atlantic and the Western Mediterranean Sea. *J. Geophys. Res. Oceans*
 931 **123**: 5481-5499. <https://doi.org/10.1029/2018JC014211>

932 Elbaz-Poulitchet, F., G. Cauwet, D. M. Guan, D. Faguet, R. Barlow, and R. F. C. Mantoura. 1994.
 933 C18 Sep-Pak extractable trace metals in waters from the Gulf of Lions. *Mar. Chem.* **46**:
 934 67-75. [https://doi.org/10.1016/0304-4203\(94\)90046-9](https://doi.org/10.1016/0304-4203(94)90046-9)

935 Ertel, J. R., J. I. Hedges, A. H. Devol, J. E. Richey, and M. d. N. G. Ribeiro. 1986. Dissolved humic
 936 substances of the Amazon River system 1. *Limnol. Oceanogr.* **31**: 739-754.
 937 <https://doi.org/10.4319/lo.1986.31.4.0739>

938 Gledhill, M., E. P. Achterberg, K. Li, K. N. Mohamed, and M. J. A. Rijkenberg. 2015. Influence of
 939 ocean acidification on the complexation of iron and copper by organic ligands in
 940 estuarine waters. *Mar. Chem.* **177**: 421-433.
 941 <https://doi.org/10.1016/j.marchem.2015.03.016>

942 Green, N. W., E. M. Perdue, G. R. Aiken, *et al.* 2014. An intercomparison of three methods for
 943 the large-scale isolation of oceanic dissolved organic matter. *Mar. Chem.* **161**: 14-19.
 944 <https://doi.org/10.1016/j.marchem.2014.01.012>

945 Guimberteau, M., J. Ronchail, J. C. Espinoza, *et al.* 2013. Future changes in precipitation and
 946 impacts on extreme streamflow over Amazonian sub-basins. *Environ. Res. Lett.* **8**:
 947 014035. <http://dx.doi.org/10.1088/1748-9326/8/1/014035>

948 Guinoiseau, D., J. Bouchez, A. Gélabert, *et al.* 2018. Fate of particulate copper and zinc isotopes
 949 at the Solimões-Negro river confluence, Amazon Basin, Brazil. *Chem. Geol.* **489**: 1-15.
 950 <https://doi.org/10.1016/j.chemgeo.2018.05.004>

951 Hamilton-Taylor, J., A. S. Postill, E. Tipping, and M. P. Harper. 2002. Laboratory measurements
 952 and modeling of metal-humic interactions under estuarine conditions. *Geochim.*
 953 *Cosmochim. Acta.* **66**: 403-415. [https://doi.org/10.1016/S0016-7037\(01\)00777-3](https://doi.org/10.1016/S0016-7037(01)00777-3)

954 Hawkes, J. A., P. J. R. Sjöberg, J. Bergquist, and L. J. Tranvik. 2019. Complexity of dissolved
 955 organic matter in the molecular size dimension: insights from coupled size exclusion
 956 chromatography electrospray ionisation mass spectrometry. *Faraday Discuss.* **218**: 52-
 957 71. <https://doi.org/10.1039/C8FD00222C>

958 Heidari, M. 2019. Role of natural flocculation in eliminating toxic metals. *Arch. Environ. Con.*
 959 *Tox.* **76**: 366-374. <https://doi.org/10.1007/s00244-019-00597-x>

960 Illuminati, S., A. Annibaldi, C. Truzzi, *et al.* 2019. In-situ trace metal (Cd, Pb, Cu) speciation along
 961 the Po River plume (Northern Adriatic Sea) using submersible systems. *Mar. Chem.* **212**:
 962 47-63. <https://doi.org/10.1016/j.marchem.2019.04.001>

963 Jacquot, J. E., and J. W. Moffett. 2015. Copper distribution and speciation across the
 964 International GEOTRACES Section GA03. *Deep Sea Res. Part II Top. Stud. Ocenogr.* **116**:
 965 187-207. <https://doi.org/10.1016/j.dsr2.2014.11.013>

966 Kogut, M. B., and B. M. Voelker. 2001. Strong copper-binding behavior of terrestrial humic
 967 substances in seawater. *Environ. Sci. Technol.* **35**: 1149-1156.
 968 <https://doi.org/10.1021/es0014584>

969 Koschinsky, A., F. Frank, T. Dittmar, *et al.* 2018. Interactions of trace metals, DOM, and particles
 970 in the Amazon estuary and associated plume as key processes for trace metal and DOM

971 fluxes into the Atlantic. METEOR-Berichte. Alemanha.[Cruise M147], p. 1-63.
 972 https://doi.org/10.2312/cr_m147

973 Ksionzek, K. B., J. Zhang, K-U. Ludwiczowski, *et al.* 2018. Stoichiometry, polarity, and
 974 organometallics in solid-phase extracted dissolved organic matter of the Elbe-Weser
 975 estuary. PloS one **13**: e0203260. <https://doi.org/10.1371/journal.pone.0203260>

976 Lacerda, L. D., M. de Souza, and M. G. Ribeiro. 2004. The effects of land use change on mercury
 977 distribution in soils of Alta Floresta, Southern Amazon. Environ. Pollut. **129**: 247-255.
 978 <https://doi.org/10.1016/j.envpol.2003.10.013>

979 Laglera, L. M., C. Sukekava, H. A. Slagter, J. Downes, A. Aparicio-Gonzalez, and L. J. A. Gerringa.
 980 2019. First quantification of the controlling role of humic substances in the transport of
 981 iron across the surface of the Arctic Ocean. Environ. Sci. Technol. **53**: 13136-13145.
 982 <https://doi.org/10.1021/acs.est.9b04240>

983 Laglera, L. M., and A. Tovar-Sánchez. 2012. Direct recognition and quantification by voltammetry
 984 of thiol/thioamide mixes in seawater. Talanta **89**: 496-504.
 985 <https://doi.org/10.1016/j.talanta.2011.12.075>

986 Laglera, L. M., and C. M. G. van den Berg. 2003. Copper complexation by thiol compounds in
 987 estuarine waters. Mar. Chem. **82**: 71-89. <https://doi.org/10.1023/A:1009903824243>

988 ---. 2009. Evidence for geochemical control of iron by humic substances in seawater. Limnol.
 989 Oceanogr. **54**: 610-619. <https://doi.org/10.4319/lo.2009.54.2.0610>

990 Lara, R. J., and T. Dittmar. 1999. Nutrient dynamics in a mangrove creek (North Brazil) during the
 991 dry season. Mangroves and Salt Marshes **3**: 185-195.
 992 <https://doi.org/10.1023/A:1009903824243>

993 Leal, M. F. C., M. T. S. D. Vasconcelos, and C. M. van den Berg. 1999. Copper-induced release of
 994 complexing ligands similar to thiols by *Emiliana huxleyi* in seawater cultures. *Limnol.*
 995 *Oceanogr.* **44**: 1750-1762. <https://doi.org/10.4319/lo.1999.44.7.1750>
 996 Lodeiro, P., C. Rey-Castro, C. David, E. P. Achterberg, J. Puy, and M. Gledhill. 2020. Acid-base
 997 properties of dissolved organic matter extracted from the marine environment. *Sci.*
 998 *Total Environ.*: 138437. <https://doi.org/10.1016/j.scitotenv.2020.138437>
 999 Lorenzo, J. I., M. Nieto-Cid, X. A. Álvarez-Salgado, P. Pérez, and R. Beiras. 2007. Contrasting
 1000 complexing capacity of dissolved organic matter produced during the onset,
 1001 development and decay of a simulated bloom of the marine diatom *Skeletonema*
 1002 *costatum*. *Mar. Chem.* **103**: 61-75. <https://doi.org/10.1016/j.marchem.2006.05.009>
 1003 Mantoura, R. F. C., A. Dickson, and J. P. Riley. 1978. The complexation of metals with humic
 1004 materials in natural waters. *Estuar. Coast. Mar. Sci.* **6**: 387-408.
 1005 [https://doi.org/10.1016/0302-3524\(78\)90130-5](https://doi.org/10.1016/0302-3524(78)90130-5)
 1006 McKnight, D. M., and G. R. Aiken. 1998. Sources and age of aquatic humus, p. 9-39. *Aquatic*
 1007 *humic substances*. Springer.
 1008 Medeiros, P. M., M. Seidel, N. D. Ward, *et al.* 2015. Fate of the Amazon River dissolved organic
 1009 matter in the tropical Atlantic Ocean. *Global Biogeochem. Cycles* **29**: 677-690.
 1010 <https://doi.org/10.1002/2015GB005115>
 1011 Mellett, T., M. T. Brown, P. D. Chappell, *et al.* 2018. The biogeochemical cycling of iron, copper,
 1012 nickel, cadmium, manganese, cobalt, lead, and scandium in a California Current
 1013 experimental study. *Limnol. Oceanogr.* **63**: S425-S447.
 1014 <https://doi.org/10.1002/lno.10751>
 1015 Meybeck, M. 1982. Carbon, nitrogen, and phosphorus transport by world rivers. *Am. J. Sci* **282**:
 1016 401-450. <https://doi.org/10.2475/ajs.282.4.401>

1017 Moffett, J. W., and L. E. Brand. 1996. Production of strong, extracellular Cu chelators by marine
 1018 cyanobacteria in response to Cu stress. *Limnol. Oceanogr.* **41**: 388-395.
 1019 <https://doi.org/10.4319/lo.1996.41.3.0388>

1020 Moffett, J. W., and C. Dupont. 2007. Cu complexation by organic ligands in the sub-arctic NW
 1021 Pacific and Bering Sea. *Deep Sea Res. Part I Oceanogr. Res. Papers* **54**: 586-595.
 1022 <https://doi.org/10.1016/j.dsr.2006.12.013>

1023 Morel, F. M. M., and N. M. Price. 2003. The biogeochemical cycles of trace metals in the oceans.
 1024 *Science* **300**: 944-947. <https://doi.org/10.1126/science.1083545>

1025 Mosley, L. M., K. A. Hunter, and W. A. Ducker. 2003. Forces between colloid particles in natural
 1026 waters. *Environ. Sci. Technol.* **37**: 3303-3308. <https://doi.org/10.1021/es026216d>

1027 Mosley, L. M., and P. S. Liss. 2020. Particle aggregation, pH changes and metal behaviour during
 1028 estuarine mixing: review and integration. *Mar. Freshwater Res.* **71**: 300-310.
 1029 <https://doi.org/10.1071/MF19195>

1030 Muller, F. L. L., and S. Batchelli. 2013. Copper binding by terrestrial versus marine organic ligands
 1031 in the coastal plume of River Thurso, North Scotland. *Estuar. Coast. Shelf Sci.* **133**: 137-
 1032 146. <https://doi.org/10.1016/j.ecss.2013.08.024>

1033 Muller, F. L. L., and M. Cuscov. 2017. Alteration of the copper-binding capacity of iron-rich humic
 1034 colloids during transport from peatland to marine waters. *Environ. Sci. Technol.* **51**:
 1035 3214-3222. <https://doi.org/10.1021/acs.est.6b05303>

1036 Nixon, R. L., S. L. Jackson, J. T. Cullen, and A. R. S. Ross. 2019. Distribution of copper-complexing
 1037 ligands in Canadian Arctic waters as determined by immobilized copper (II)-ion affinity
 1038 chromatography. *Mar. Chem.* **215**: 103673.
 1039 <https://doi.org/10.1016/j.marchem.2019.103673>

1040 Omanović, D., C. Garnier, and I. Pižeta. 2015. ProMCC: an all-in-one tool for trace metal
 1041 complexation studies. *Mar. Chem.* **173**: 25-39.
 1042 <https://doi.org/10.1016/j.marchem.2014.10.011>
 1043 Pavoni, E., M. Crosera, E. Petranich, G. Adami, J. Faganeli, and S. Covelli. 2020. Partitioning and
 1044 mixing behaviour of trace elements at the Isonzo/Soča River mouth (Gulf of Trieste,
 1045 northern Adriatic Sea). *Mar. Chem.* **223**: 103800.
 1046 <https://doi.org/10.1016/j.marchem.2020.103800>
 1047 Pearson, H. B. C., S. D. W. Comber, C. Braungardt, and P. J. Worsfold. 2017. Predicting Copper
 1048 Speciation in Estuarine Waters: Is Dissolved Organic Carbon a Good Proxy for the
 1049 Presence of Organic Ligands? *Environ. Sci. Technol.* **51**: 2206-2216.
 1050 <https://doi.org/10.1021/acs.est.6b05510>
 1051 Peers, G., S. A. Quesnel, and N. M. Price. 2005. Copper requirements for iron acquisition and
 1052 growth of coastal and oceanic diatoms. *Limnol. Oceanogr.* **50**: 1149-1158.
 1053 <https://doi.org/10.4319/lo.2005.50.4.1149>
 1054 Perminova, I. V., F. H. Frimmel, A. V. Kudryavtsev, *et al.* 2003. Molecular weight characteristics
 1055 of humic substances from different environments as determined by size exclusion
 1056 chromatography and their statistical evaluation. *Environ. Sci. Technol.* **37**: 2477-2485.
 1057 <https://doi.org/10.1021/es0258069>
 1058 Posacka, A. M., D. M. Semeniuk, H. Whitby, *et al.* 2017. Dissolved copper (dCu) biogeochemical
 1059 cycling in the subarctic Northeast Pacific and a call for improving methodologies. *Mar.*
 1060 *Chem.* **196**: 47-61. <https://doi.org/10.1016/j.marchem.2017.05.007>
 1061 Raeke, J., O. J. Lechtenfeld, M. Wagner, P. Herzsprung, and T. Reemtsma. 2016. Selectivity of
 1062 solid phase extraction of freshwater dissolved organic matter and its effect on ultrahigh

1063 resolution mass spectra. Environ. Sci-Proc. Imp. **18**: 918-927.

1064 <https://doi.org/10.1039/C6EM00200E>

1065 Rapp, I., C. Schlosser, D. Rusiecka, M. Gledhill, and E. P. Achterberg. 2017. Automated

1066 preconcentration of Fe, Zn, Cu, Ni, Cd, Pb, Co, and Mn in seawater with analysis using

1067 high-resolution sector field inductively-coupled plasma mass spectrometry. Anal. Chim.

1068 Acta. **976**: 1-13. <https://doi.org/10.1016/j.aca.2017.05.008>

1069 Richey, J. E., R. H. Meade, E. Salati, A. H. Devol, C. F. Nordin Jr, and U. D. Santos. 1986. Water

1070 discharge and suspended sediment concentrations in the Amazon River: 1982–1984.

1071 Water Resour. Res. **22**: 756-764. <https://doi.org/10.1029/WR022i005p00756>

1072 Rodrigues Filho, S., and J. E. L. Maddock. 1997. Mercury pollution in two gold mining areas of

1073 the Brazilian Amazon. J. Geochem. Explor. **58**: 231-240. [https://doi.org/10.1016/S0375-](https://doi.org/10.1016/S0375-6742(97)00006-X)

1074 [6742\(97\)00006-X](https://doi.org/10.1016/S0375-6742(97)00006-X)

1075 Santos-Echeandía, J., M. Caetano, L. M. Laglera, and C. Vale. 2013. Salt-marsh areas as copper

1076 complexing ligand sources to estuarine and coastal systems. Chemosphere **90**: 772-781.

1077 <https://doi.org/10.1016/j.chemosphere.2012.09.074>

1078 Sarbolouki, M. N. 1982. A general diagram for estimating pore size of ultrafiltration and reverse

1079 osmosis membranes. Sep. Sci. Technol. **17**: 381-386.

1080 <https://doi.org/10.1080/01496398208068547>

1081 Semeniuk, D. M., J. T. Cullen, W. K. Johnson, K. Gagnon, T. J. Ruth, and M. T. Maldonado. 2009.

1082 Plankton copper requirements and uptake in the subarctic Northeast Pacific Ocean.

1083 Deep Sea Res. Part I Oceanogr. Res. Papers **56**: 1130-1142.

1084 <https://doi.org/10.1016/j.dsr.2009.03.003>

1085 Seyler, P. T., and G. R. Boaventura. 2003. Distribution and partition of trace metals in the

1086 Amazon basin. Hydrol. Process. **17**: 1345-1361. <https://doi.org/10.1002/hyp.1288>

1087 Shank, G. C., S. A. Skrabal, R. F. Whitehead, and R. J. Kieber. 2004. Strong copper complexation
 1088 in an organic-rich estuary: the importance of allochthonous dissolved organic matter.
 1089 Mar. Chem. **88**: 21-39. <https://doi.org/10.1016/j.marchem.2004.03.001>
 1090 Sholkovitz, E. R. 1976. Flocculation of dissolved organic and inorganic matter during the mixing
 1091 of river water and seawater. Geochim. Cosmochim. Acta. **40**: 831-845.
 1092 [https://doi.org/10.1016/0016-7037\(76\)90035-1](https://doi.org/10.1016/0016-7037(76)90035-1)
 1093 Smoak, J. M., J. M. Krest, and P. W. Swarzenski. 2006. Geochemistry of the Amazon estuary, p.
 1094 71-90. Estuaries. Springer.
 1095 Sunda, W. 2012. Feedback interactions between trace metal nutrients and phytoplankton in the
 1096 ocean. Front. Microbiol. **3**: 204-226. <https://doi.org/10.3389/fmicb.2012.00204>
 1097 Tang, D., K. W. Warnken, and P. H. Santschi. 2001. Organic complexation of copper in surface
 1098 waters of Galveston Bay. Limnol. Oceanogr. **46**: 321-330.
 1099 <https://doi.org/10.4319/lo.2001.46.2.0321>
 1100 ---. 2002. Distribution and partitioning of trace metals (Cd, Cu, Ni, Pb, Zn) in Galveston bay
 1101 waters. Mar. Chem. **78**: 29-45. [https://doi.org/10.1016/S0304-4203\(02\)00007-5](https://doi.org/10.1016/S0304-4203(02)00007-5)
 1102 Town, R. M., and M. Filella. 2000a. A comprehensive systematic compilation of complexation
 1103 parameters reported for trace metals in natural waters. Aquat. Sci. **62**: 252-295.
 1104 <https://doi.org/10.1007/PL00001335>
 1105 ---. 2000b. Dispelling the myths: Is the existence of L1 and L2 ligands necessary to explain metal
 1106 ion speciation in natural waters? Limnol. Oceanogr. **45**: 1341-1357.
 1107 <https://doi.org/10.4319/lo.2000.45.6.1341>
 1108 van den Berg, C. M. G., A. G. A. Merks, and E. K. Duursma. 1987. Organic complexation and its
 1109 control of the dissolved concentrations of copper and zinc in the Scheldt estuary. Estuar.
 1110 Coast. Shelf Sci. **24**: 785-797. [https://doi.org/10.1016/0272-7714\(87\)90152-1](https://doi.org/10.1016/0272-7714(87)90152-1)

1111 Van Heukelem, L., and C. S. Thomas. 2001. Computer-assisted high-performance liquid
 1112 chromatography method development with applications to the isolation and analysis of
 1113 phytoplankton pigments. *J. Chromatogr. A.* **910**: 31-49. [https://doi.org/10.1016/S0378-](https://doi.org/10.1016/S0378-4347(00)00603-4)
 1114 [4347\(00\)00603-4](https://doi.org/10.1016/S0378-4347(00)00603-4)
 1115 Villar, J. C. E., J. L. Guyot, J. Ronchail, *et al.* 2009. Contrasting regional discharge evolutions in the
 1116 Amazon basin (1974–2004). *J. Hydrol.* **375**: 297-311.
 1117 <https://doi.org/10.1016/j.jhydrol.2009.03.004>
 1118 Voelker, B. M., and M. B. Kogut. 2001. Interpretation of metal speciation data in coastal waters:
 1119 the effects of humic substances on copper binding as a test case. *Mar. Chem.* **74**: 303-
 1120 318. [https://doi.org/10.1016/S0304-4203\(01\)00022-6](https://doi.org/10.1016/S0304-4203(01)00022-6)
 1121 Waska, H., A. Koschinsky, M. J. R. Chanco, and T. Dittmar. 2015. Investigating the potential of
 1122 solid-phase extraction and Fourier-transform ion cyclotron resonance mass
 1123 spectrometry (FT-ICR-MS) for the isolation and identification of dissolved metal–organic
 1124 complexes from natural waters. *Mar. Chem.* **173**: 78-92.
 1125 <https://doi.org/10.1016/j.marchem.2014.10.001>
 1126 Wells, M. L., P. B. Kozelka, and K. W. Bruland. 1998. The complexation of 'dissolved' Cu, Zn, Cd
 1127 and Pb by soluble and colloidal organic matter in Narragansett Bay, RI. *Mar. Chem.* **62**:
 1128 203-217. [https://doi.org/10.1016/S0304-4203\(98\)00041-3](https://doi.org/10.1016/S0304-4203(98)00041-3)
 1129 Whitby, H., J. T. Hollibaugh, and C. M. van den Berg. 2017. Chemical speciation of copper in a
 1130 salt marsh estuary and bioavailability to Thaumarchaeota. *Front. Mar. Sci.* **4**: 178.
 1131 <https://doi.org/10.3389/fmars.2017.00178>
 1132 Whitby, H., H. Planquette, N. Cassar, *et al.* 2020. A call for refining the role of humic-like
 1133 substances in the oceanic iron cycle. *Sci. Rep.* **10**: 6144.
 1134 <https://doi.org/10.1038/s41598-020-62266-7>

1135 Whitby, H., A. M. Posacka, M. T. Maldonado, and C. M. van den Berg. 2018. Copper-binding
 1136 ligands in the NE Pacific. *Mar. Chem.* **204**: 36-48.
 1137 <https://doi.org/10.1016/j.marchem.2018.05.008>
 1138 Whitby, H., and C. M. van den Berg. 2015. Evidence for copper-binding humic substances in
 1139 seawater. *Mar. Chem.* **173**: 282-290. <https://doi.org/10.1016/j.marchem.2014.09.011>
 1140 Wilkinson, K. J., J.-C. Negre, and J. Buffle. 1997. Coagulation of colloidal material in surface
 1141 waters: the role of natural organic matter. *J. Contam. Hydrol.* **26**: 229-243.
 1142 [https://doi.org/10.1016/S0169-7722\(96\)00071-X](https://doi.org/10.1016/S0169-7722(96)00071-X)
 1143 Windom, H., R. Smith Jr, C. Rawlinson, M. Hungspreugs, S. Dharmvanij, and G. Wattayakorn.
 1144 1988. Trace metal transport in a tropical estuary. *Mar. Chem.* **24**: 293-305.
 1145 [https://doi.org/10.1016/0304-4203\(88\)90037-0](https://doi.org/10.1016/0304-4203(88)90037-0)
 1146 Wong, K. H., H. Obata, T. Kim, Y. Wakuta, and S. Takeda. 2019. Distribution and speciation of
 1147 copper and its relationship with FDOM in the East China Sea. *Mar. Chem.* **212**: 96-107.
 1148 <https://doi.org/10.1016/j.marchem.2019.04.005>
 1149 Woods, G. C., M. J. Simpson, B. P. Kelleher, M. McCaul, W. L. Kingery, and A. J. Simpson. 2010.
 1150 Online high-performance size exclusion chromatography– nuclear magnetic resonance
 1151 for the characterization of dissolved organic matter. *Environ. Sci. Technol.* **44**: 624-630.
 1152 <https://doi.org/10.1021/es903042s>
 1153 Yamasoe, M. A., P. Artaxo, A. H. Miguel, and A. G. Allen. 2000. Chemical composition of aerosol
 1154 particles from direct emissions of vegetation fires in the Amazon Basin: water-soluble
 1155 species and trace elements. *Atmos. Environ.* **34**: 1641-1653.
 1156 [https://doi.org/10.1016/S1352-2310\(99\)00329-5](https://doi.org/10.1016/S1352-2310(99)00329-5)
 1157 Zhang, J. 1995. Geochemistry of trace metals from Chinese river/estuary systems: an overview.
 1158 *Estuar. Coast. Shelf Sci.* **41**: 631-658. <https://doi.org/10.1006/ecss.1995.0082>

1159 Zhang, Z., Z. Cao, P. Grasse, *et al.* 2020. Dissolved silicon isotope dynamics in large river
1160 estuaries. *Geochim. Cosmochim. Acta.* **273**: 367-382.
1161 <https://doi.org/10.1016/j.gca.2020.01.028>
1162 Zigah, K. P., A. P. McNichol, L. Xu, *et. al.* 2017. Allochthonous sources and dynamic cycling of
1163 ocean dissolved organic carbon revealed by carbon isotopes. *Geophys. Res. Lett.* **44**:
1164 2407-2415. <https://doi.org/10.1002/2016GL071348>
1165

Acknowledgments

We thank Rebecca Zitoun, Sophie Paul and Luise Heinrich for sample management in the clean container and in the ship's lab and the captain and crew of RV Meteor for their help and support during the cruise. We thank A. Mutzberg for the nutrient analysis, K. Nachtigall for HPLC analysis of chlorophyll *a* and T. Steffens and D. Jasinski for their assistance with ICP-MS analysis. Thank you also to Thorsten Dittmar (ICBM) and Melina Knoke (ICBM) for their support with DOM analysis. Thank you also to our Brazilian partners, specifically Carlos Rezende (UENF) and Fabiano Thompson (UFRJ), and to the Brazilian government (Ministério da Marinha) for the opportunity to sample in the Brazil exclusive economic zone (EEZ). Finally, thank you to two anonymous reviewers for their insightful comments on the manuscript. A.H. and P.L. were supported by Grant Nos. KO 2906/13-1 and GL 807/2-1, respectively, from the German Science Foundation DFG (Deutsche Forschungsgemeinschaft). P.L. is also supported by a Beatriz Galindo Senior Fellowship (BG20/00104) from Ministerio de Ciencia, Innovación y Universidades of Spain, and University of Lleida. DFG is also acknowledged for funding R/V Meteor cruise M147.

Tables

Table 1. Cu concentrations (nmol L⁻¹) of CASS 6 and NASS 7 standard (National Research Council Canada (NRC-CNRC)), quality control (QC) South Atlantic seawater and manifold (air) blank. Samples were analyzed by inductively coupled plasma-mass spectrometry (ICP-MS) following seaFAST preconcentration. Concentrations were determined using isotope dilution for all samples except manifold blanks, which were determined using standard curves and dividing by the seaFAST preconcentration factor. Error is reported as the standard deviation of analytical replicates. Reference values and errors are reported by NRC-CNRC. The limit of detection (LOD) is three times manifold blank standard deviation.

	Cu measured value, nmol L ⁻¹	Cu reference value, nmol L ⁻¹	Limit of detection, pmol L ⁻¹
CASS 6	8.58±0.22 (n=9)	8.18±0.50	NA
NASS 7	2.94±0.09 (n=5)	3.13±0.22	NA
QC	11.96±0.64 (n=7)	NA	NA
Manifold blank	0.0023±0.0017 (n=30)	NA	5.2

Table 2. Linear regression analyses for dissolved (<0.2 µm) and soluble (<0.015 µm) Cu (nmol L⁻¹) versus salinity in the Amazon Transect, Pará Transect, Plume North, Mangrove Belt and North Brazil Current. For the North Brazil Current dissolved and soluble fractions, no statistically significant trend was observed.

	Slope, Cu (nmol L ⁻¹) per unit salinity	Intercept, Cu (nmol L ⁻¹) per unit salinity	<i>n</i>	R	<i>p</i>
Dissolved Cu, <0.2 µm					
Amazon Transect	-0.68±0.05	23.4±0.8	38	0.83	<0.0001
Pará Transect	-0.46±0.04	17.0±0.8	14	0.95	<0.0001
Plume North	-0.60±0.06	21.6±1.0	14	0.94	<0.0001
Mangrove Belt	-0.37±0.04	14.6±1.3	20	0.91	<0.0001
North Brazil Current	0.09±0.25	-2.4±9.0	16	0.21	0.4
Soluble Cu, <0.015 µm					
Amazon Transect	-0.41±0.06	18.5±0.9	29	0.82	<0.0001
Pará Transect	-0.24±0.03	13.9±0.4	8	0.96	0.0002
Plume North	-0.44±0.05	18.4±0.80	13	0.94	<0.0001
Mangrove Belt	-0.51±0.15	20.3±4.6	15	0.69	0.004
North Brazil Current	1.25±1.38	-42.3±49.2	7	0.37	0.4

1202 Figures

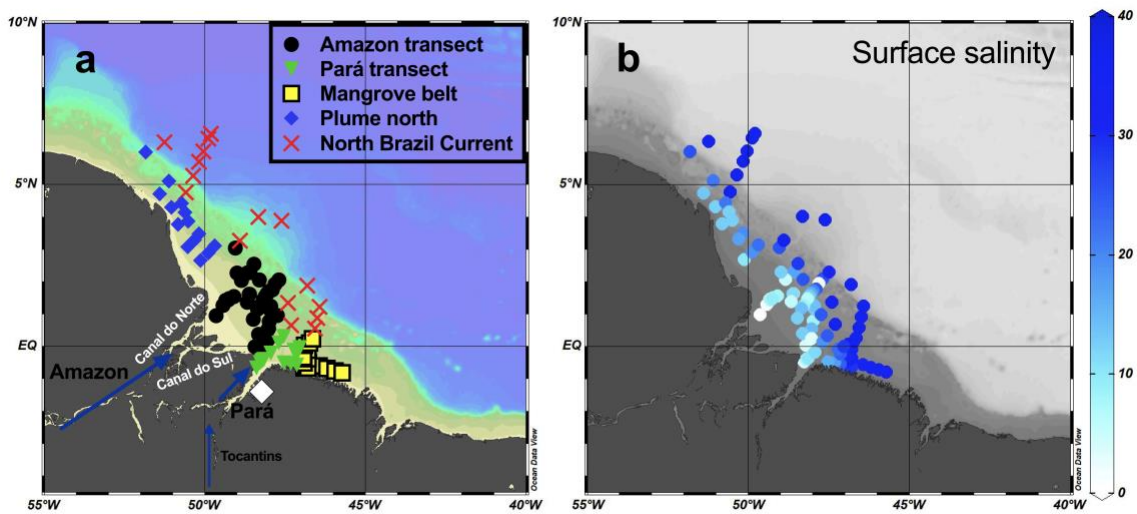


Figure 1. Sample group assignments (a) and salinity data (b) for surface samples plotted in Ocean Data View (ODV). Designations for towed-fish sample groups correspond to the Amazon River Transect (black circle), Pará River Transect (green inverted triangle), Mangrove Belt (yellow square), plume aging northward (“Plume north”; blue diamond) and North Brazil Current (NBC; red X). Belém, the starting point of the cruise, is represented by the white diamond.

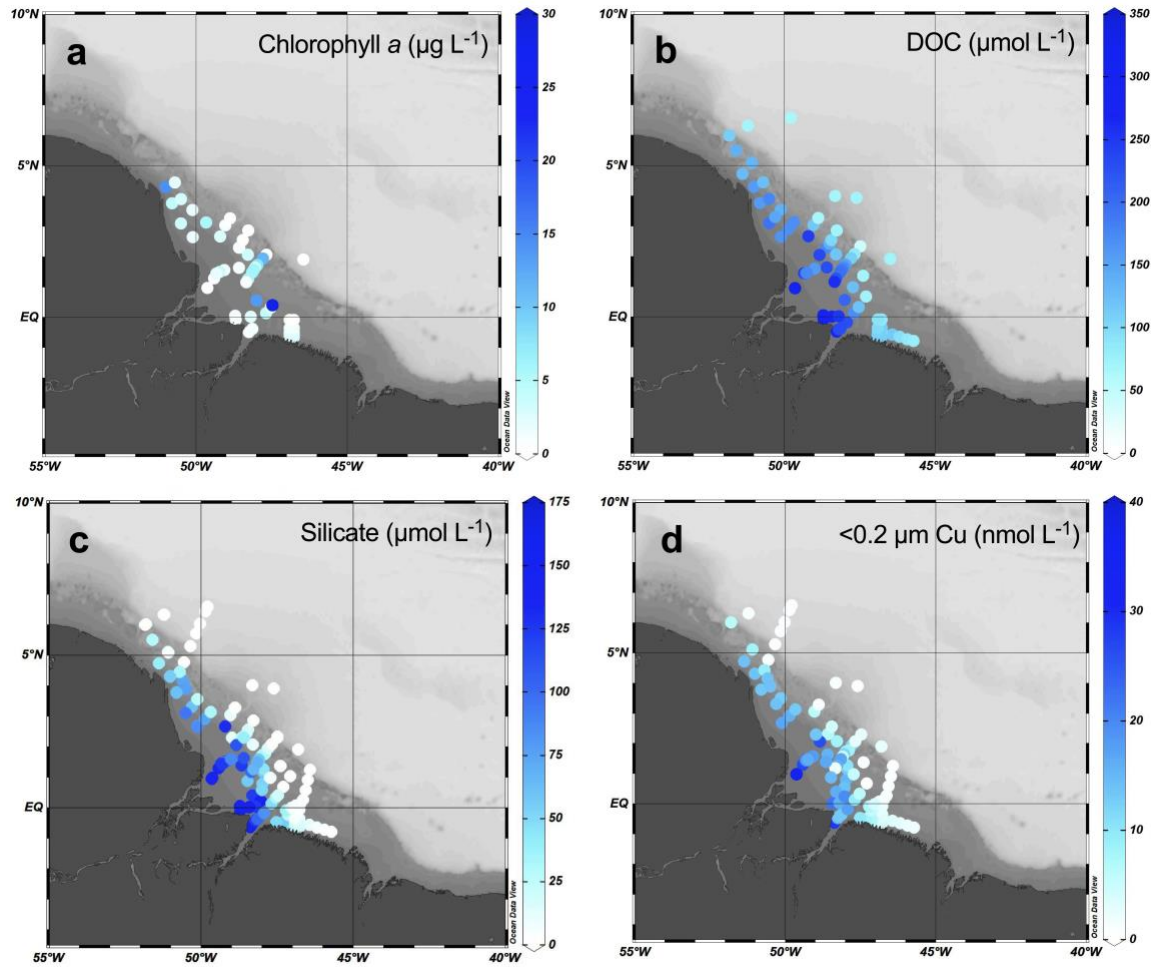


Figure 2. Ocean data view (ODV) plots of chlorophyll *a*, (Chl *a*, $\mu\text{g L}^{-1}$, **a**), dissolved organic carbon (DOC, $\mu\text{mol L}^{-1}$, **b**), silicate ($\mu\text{mol L}^{-1}$, **c**), and dissolved copper (Cu, nmol L^{-1} , **d**).

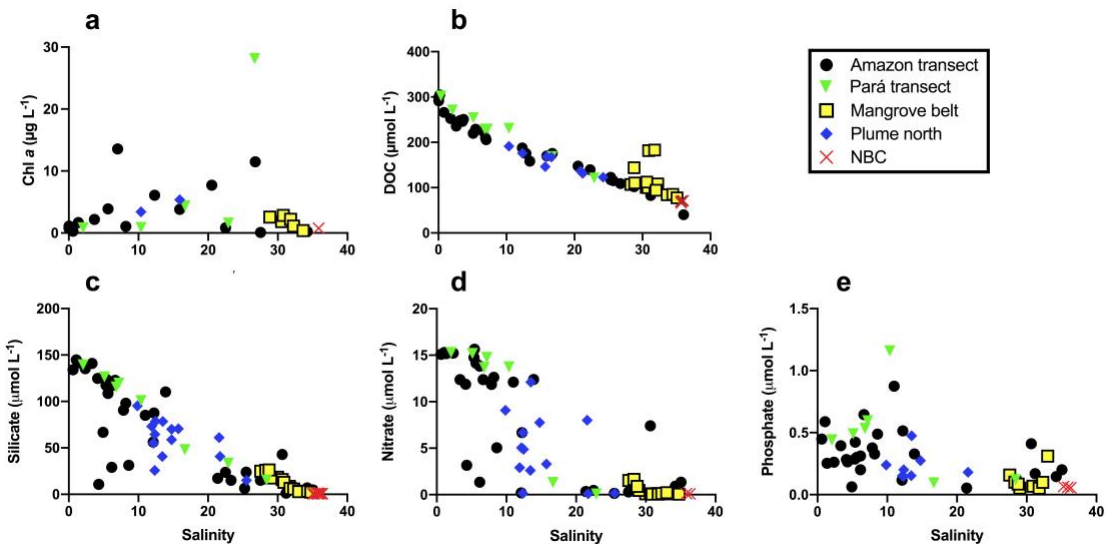


Figure 3. Concentrations of chlorophyll *a*, (Chl *a*, $\mu\text{g L}^{-1}$, **a**), dissolved organic carbon (DOC, $\mu\text{mol L}^{-1}$, **b**), silicate ($\mu\text{mol L}^{-1}$, **c**), nitrate ($\mu\text{mol L}^{-1}$, **d**) and phosphate ($\mu\text{mol L}^{-1}$, **e**) plotted against salinity.

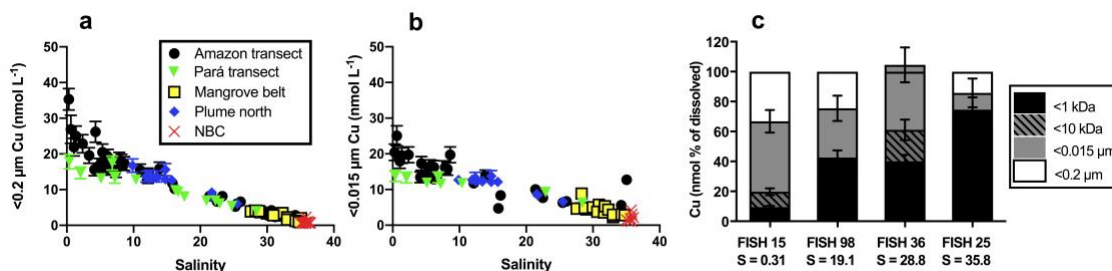


Figure 4. Concentration of Cu (nmol L^{-1}) plotted against salinity for the dissolved ($<0.2 \mu\text{m}$, **a**) and soluble ($<0.015 \mu\text{m}$, **b**) size fractions. A bar graph (**c**) shows size comparison (expressed as percent of total) for the four samples that were ultrafiltered at <1 and $<10 \text{ kDa}$. Concentrations in **c** (FISH 15, 98, 36 and 25) were measured from separate aliquots taken from the L_{Cu} samples, since no ultrafiltration was performed on the samples collected for trace metal analysis. Error bars are expressed as 11.2% of total, which was

estimated to be the average measurement uncertainty using the Nordtest approach.

Error bars that are smaller than the symbol size are not visible on the graphs.

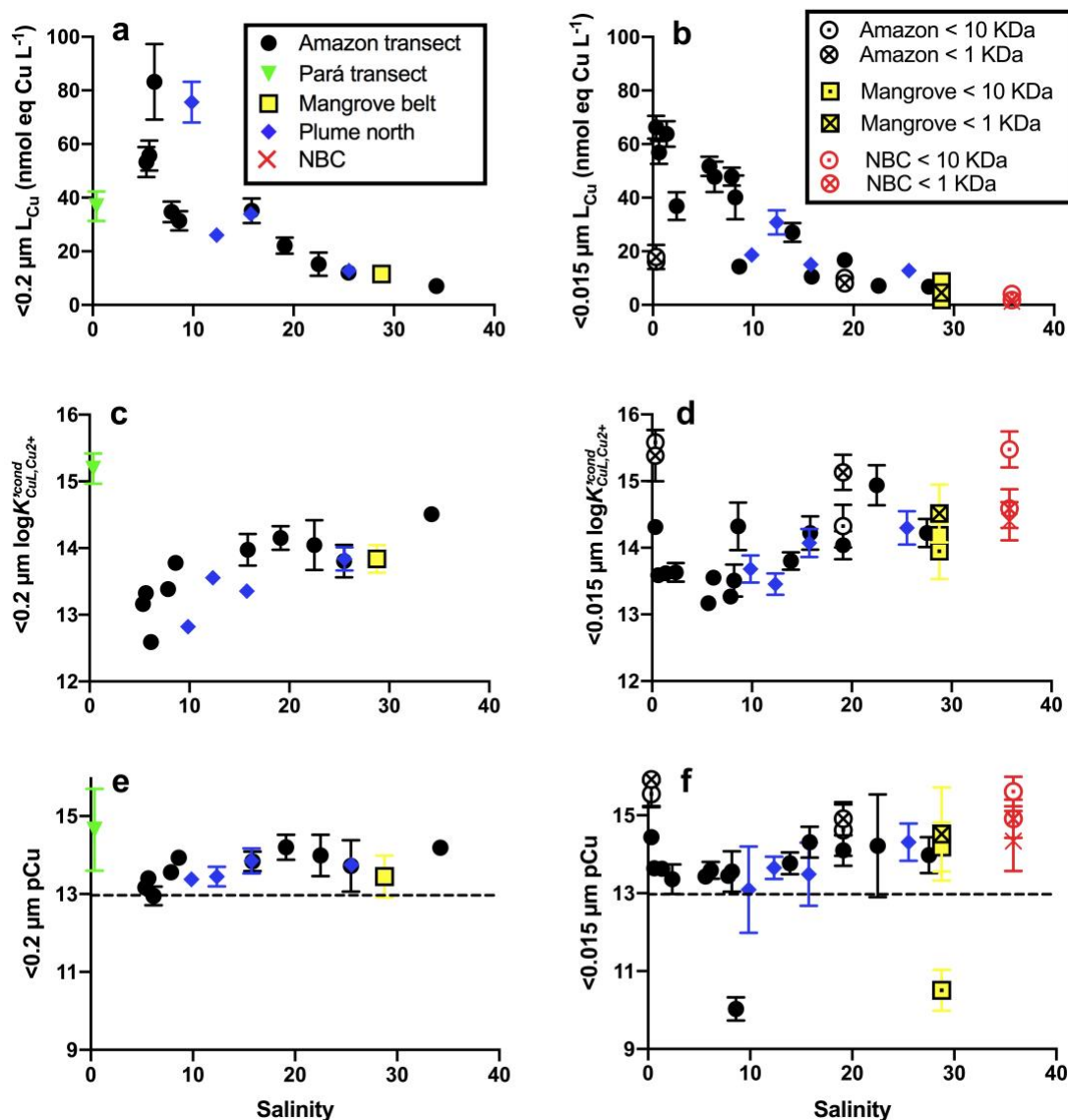


Figure 5. Apparent Cu binding organic ligands (L_{Cu} , nmol eq Cu L^{-1} , **a-b**), conditional stability constants ($K'^{\text{cond}}_{\text{CuL}, \text{Cu}^{2+}}$, **c-d**) and pCu (defined as $-\log \text{Cu}^{2+}$ in moles L^{-1} **e-f**) plotted against salinity for dissolved ($<0.2 \mu\text{m}$, left) and soluble ($<0.015 \mu\text{m}$, right) fractions. In **e-f**, the dashed line at $\text{pCu} = 13$ denotes the threshold for possible Cu toxicity for

cyanobacteria. Ultrafiltered (UF) samples are also shown on the soluble plots as symbols with a dot (<10 KDa) or X (<1 KDa) through the middle. Error bars represent the error (95% confidence) generated from fitting the Langmuir equation in ProMCC. Error bars that are smaller than the symbol size are not visible on the graphs. The dissolved fraction of station 25 (NBC) is not shown for L_{Cu} and pCu due to high relative error (Table S1).

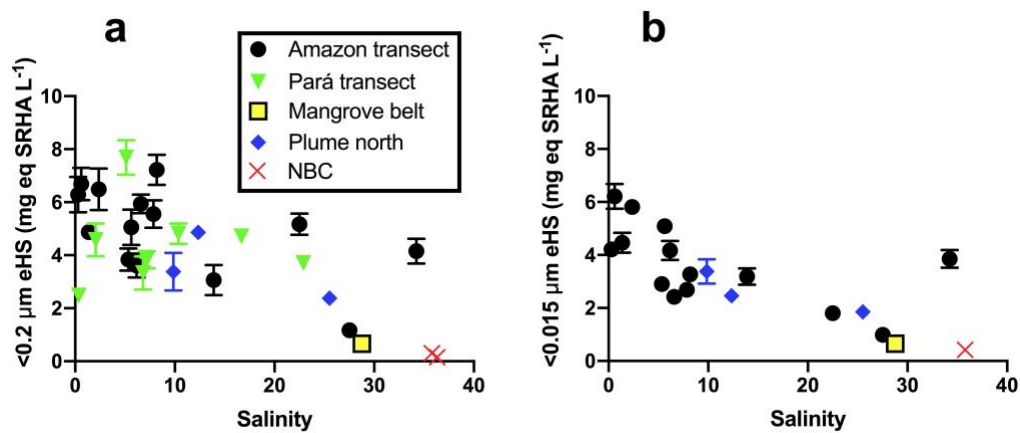


Figure 6. Electroactive humic substances (eHS, mg eq SRHA L⁻¹) plotted against salinity for dissolved (<0.2 μm, **a**) and soluble (<0.015 μm, **b**) fractions. Error bars that are smaller than the symbol size are not visible on the graphs.

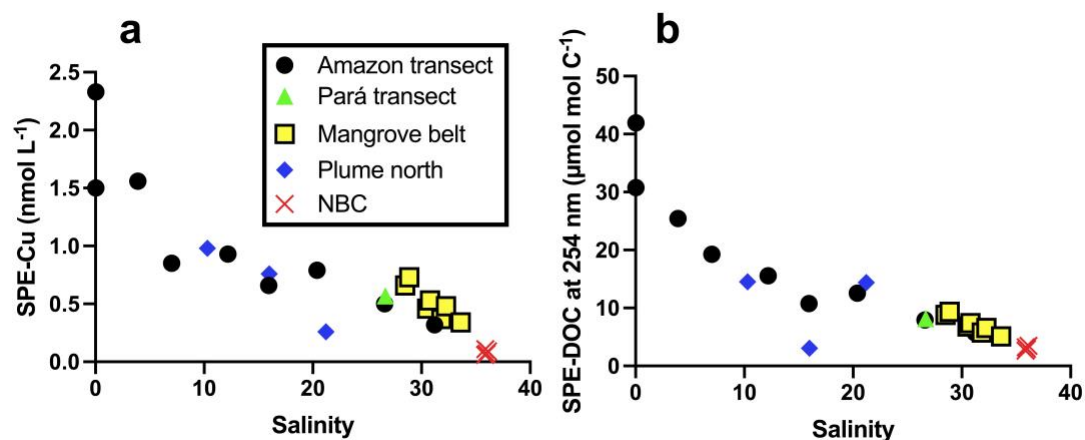


Figure 7. Solid phase extractable (SPE) Cu (SPE-Cu, nmol L⁻¹, **a**) and dissolved organic carbon at 254 nm (SPE-DOC, μmol mol C⁻¹, **b**).

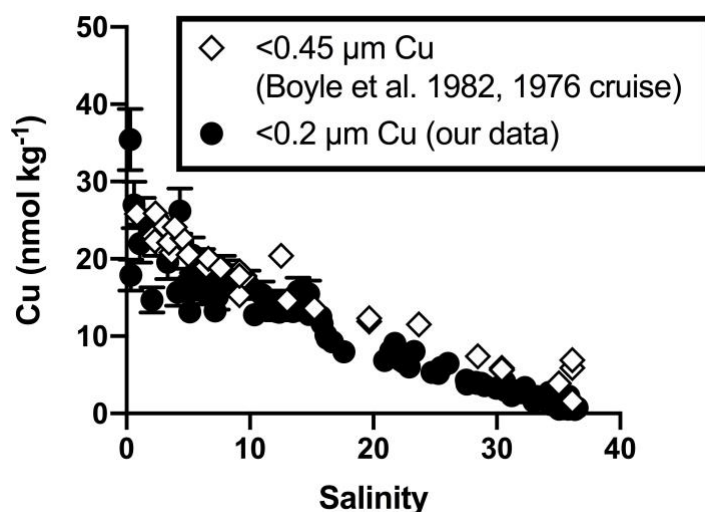


Figure 8. Dissolved Cu concentrations vs. salinity in the Amazon estuary re-plotted from Boyle et al. 1982 (1976 cruise) (nmol kg⁻¹, white diamonds), compared to data from this paper (nmol kg⁻¹, black circles).